Scilight

Nano-electrochemistry & Nano-photochemistry

https://www.sciltp.com/journals/nenp

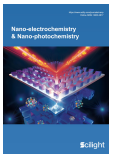

Review

Check for updates

Recent Progress on Modulation Strategies of Metal-Organic Framework-Based Catalysts for Electrochemical Carbon Dioxide Reduction

Huitong Du [1,*],Ruixin Jia [1], Xinqi Zhou [1], Ziyan Shi [1], Tianyi Wu [1], Suitao Hua [1], Rui Liu [1], Zuming Liang [1], Weisu Kong [2], Feng Han [1,*] and Chengxia Miao [1,*]

[1] Key Laboratory of Low-Carbon and Green Agriculture Chemistry in Universities of Shandong, College of Chemistry and Material Science, Shandong Agricultural University, Tai'an 271018, China

[2] College of Chemistry, Chemical Engineering and Materials Science, Key Laboratory of Molecular and Nano Probes, Ministry of Education, Collaborative Innovation Center of Functionalized Probes for Chemical Imaging in Universities of Shandong, Institute of Molecular and Nano Science, Shandong Normal University, Jinan 250014, China

* Correspondence: duhuitong@sdau.edu.cn (H.D.); fenghan@sdau.edu.cn (F.H.); chxmiao@sdau.edu.cn (C.M.)

How To Cite: Du, H.; Jia, R.; Zhou, X.; et al. Recent Progress on Modulation Strategies of Metal-Organic Framework-Based Catalysts for Electrochemical Carbon Dioxide Reduction. *Nano-electrochemistry & Nano-photochemistry* **2026**, *2*(4), 27. https://doi.org/10.53941/nenp.2026.100027

Received: 30 July 2026
Revised: 28 October 2026
Accepted: 5 November 2026
Published: 26 November 2026

Abstract: The electrochemical reduction of CO_2 offers a promising route for realizing the artificial carbon cycle by producing value-added fuels and chemical feedstocks. In the past decade, metal-organic frameworks (MOF) have emerged as the promising platform for CO_2 electrocatalyst design owing to their structural tunability, ultrahigh surface areas, and well-defined active sites. Many efforts have been devoted to the modulation of MOF-based catalysts for enhancing electrochemical CO_2 reduction performance. In this review, we present a comprehensive survey of recent advances in the design and modulation strategies of MOF-based catalysts for CO_2 electroreduction, covering intrinsic structural regulation, fabrication of MOF-based composite materials and design of MOF-derived materials. Furthermore, the prevailing challenges and future outlooks based on recent research advances are highlighted. These summarized findings and prospects afford critical references for the design of high-performance MOF-based catalysts and help further broaden the application prospect of electrocatalytic CO_2 reduction.

Keywords: metal-organic frameworks; CO_2 reduction reaction; modulation strategy; electrocatalyst; catalytic performance

1. Introduction

The continuous rise in CO_2 concentrations has driven an urgent global imperative to develop artificial carbon fixation technologies [1–5]. Among the diverse strategies, the electrochemical CO_2 reduction reaction (CO_2RR) is particularly attractive because it can be directly coupled with renewable electricity to transform intermittent electric power into stable chemical bonds, affording value-added products [6–8]. Electrocatalytic CO_2 reduction enables the conversion of CO_2 into CO, HCOOH, CH_4, CH_3OH, C_2H_4 and C_2H_5OH, etc. [9]. Notably, multi-carbon (C_{2+}) products are generally favored, as they possess higher economic value and extensive application potential [10–12]. In practice, CO_2RR encounters substantial obstacles in yielding C_{2+} products, owing to the intrinsic kinetic inertness of CO_2 molecules and favorable thermodynamic stability of reactive intermediates [13]. Furthermore, the competing hydrogen evolution reaction operates at similar potentials, reducing Faradaic efficiency (FE) toward carbonaceous products [14]. Therefore, it is of crucial importance to develop high-performance catalysts with selectivity toward C_{2+} products.

Copyright: © 2026 by the authors. This is an open access article under the terms and conditions of the Creative Commons Attribution (CC BY) license (https://creativecommons.org/licenses/by/4.0/).
Publisher's Note: Scilight stays neutral with regard to jurisdictional claims in published maps and institutional affiliations.

Metal-organic frameworks (MOF), constructed from metal ions or clusters interconnected by organic linkers, have attracted intense research interest over the past two decades [15–20]. Especially, MOF materials possess several structural attributes that make them exceptionally suited for CO_2RR. Benefiting from periodically ordered crystalline structures, MOF-based catalysts possess atomically precise and uniformly dispersed metal centers that serve as well-defined catalytic active sites, thereby establishing an ideal platform for investigating structure-activity relationships [21–24]. Their exceptional porosity and ultrahigh specific surface areas also greatly facilitate the capture and local enrichment of CO_2 around catalytic active sites [25]. Furthermore, the tremendous chemical and structural diversity realized via rational selection of metal nodes and functional modification of organic linkers offers enormous versatility for modulating the electronic structure and coordination microenvironment of catalytic centers [26–28]. Meanwhile, the well-ordered pore architectures can exert shape-selective confinement effects on reaction intermediates, providing a strategy to regulate the product selectivity of CO_2 reduction reactions [29,30]. In view of this, MOF materials have ushered in a golden age of development as high-performance catalysts for CO_2RR. A variety of modulation strategies have been proposed to develop highly active CO_2RR catalysts. These efforts not only advance the development of MOF materials, but also further broaden the application prospects of CO_2RR technology.

This review highlights the latest important regulation strategies of MOF-based electrocatalysts for CO_2RR, and briefly summarizes the advances from intrinsic modulation of MOF-based electrocatalysts, MOF-based composite electrocatalysts and MOF-derived electrocatalysts. Firstly, the typical reaction pathways of CO_2RR are introduced. Then, this review comprehensively discusses the latest advances in modulation strategies for MOF-based catalysts. Finally, the remaining research challenges and future priority directions are highlighted based on the current understandings of this field. These perspectives and insights not only offer guidance for the rational design of high-performance MOF-based electrocatalysts, but also facilitate the further development of CO_2RR technology.

2. Fundamentals of Electrochemical CO_2 Reduction Reaction

2.1. Mechanism of Electrochemical CO_2 Reduction Reaction

Mechanistic investigations into CO_2RR have emerged as a focus of research in this field, with substantial breakthroughs achieved to date. Generally, CO_2RR in aqueous media initiates with the adsorption and activation of CO_2 molecules on the electrocatalyst surface, followed by successive proton-electron transfer steps that yield a variety of reduction products [31,32]. Given the robust chemical bonding and linear molecular geometry, CO_2 exhibits exceptional stability under ambient conditions [33]. This inherent stability presents a formidable barrier to the activation of CO_2 molecules, consequently leading to sluggish reaction kinetics in electrocatalytic processes [34]. Typically, three reaction pathways have been established to describe the initial activation of CO_2 on the electrocatalyst surfaces. In one typical pathway, the carbon atom of CO_2 binds to the catalyst active site, forming an adsorbed $*CO_2^{\delta-}$ intermediate. Subsequently, the as-formed intermediate undergoes proton-electron transfer process and converts into the carbon-bound *COOH intermediate (Figure 1) [35,36]. As an alternative, CO_2 activation through oxygen coordination or mixed carbon/oxygen coordination has also been widely validated. In addition, the *COOH species generated via the aforementioned pathway can be further converted into *CO, which participates in the subsequent reduction to form deeper reduction products [37,38].

For C_1 reduction products, the generation of adsorbed *COOH and *OCHO intermediates constitutes the initial step following CO_2 activation [39,40]. Specifically, the HCOOH pathway via a single proton-electron transfer step of the *OCHO intermediate represents the most widely adopted mechanism [41]. Meanwhile, *CO is produced through the proton-electron transfer process of the *COOH intermediate and desorbed as CO gas when released from the catalyst surface. When the binding energy of *CO is moderate, this intermediate can undergo successive proton-electron transfer steps to form key *COH and *CHO intermediates, which are further reduced to yield CH_4 or CH_3OH [42,43].

For the production of C_{2+} reduction products, C-C bond formation is of paramount importance [44,45]. The prevalent pathways for C-C bond formation mainly rely on C-C coupling reactions between *CO and various C_1 intermediates [46]. For instance, the dimerization of two *CO species to form a C-C bond is widely recognized as the critical step for the generation of C_{2+} products [47]. Moreover, *CO can couple with *COH to produce the *COCOH intermediate, which is also a key intermediate toward various C_{2+} products in current study [48,49]. Following C-C bond formation, successive proton-electron transfer processes proceed continuously until the binding energy of the generated species is altered, enabling desorption from the catalyst surface and yielding various C_{2+} product [50].

This section outlines the most widely recognized reaction mechanisms for CO_2RR. Given the intricate factors involved in this reaction, the distribution of reduction products strongly depends on the catalyst, electrolyte, and applied potential, etc.

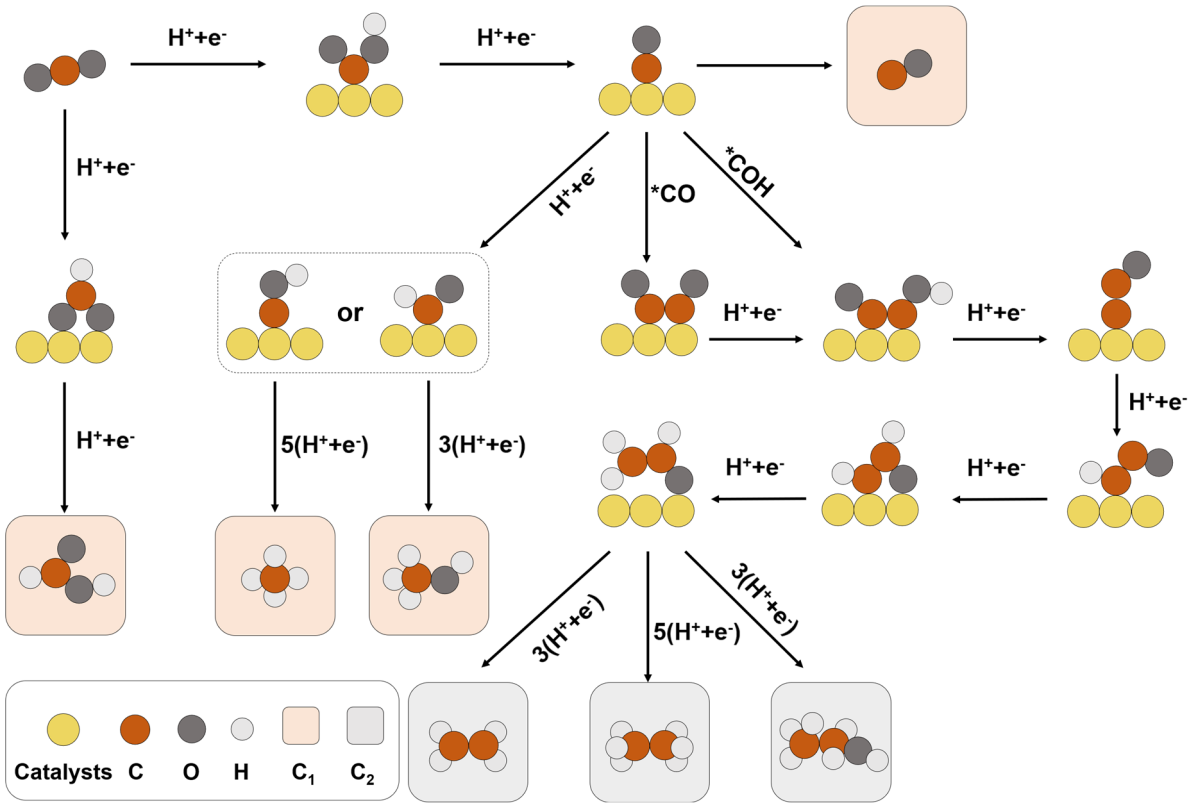

Figure 1. Possible mechanistic pathways for CO_2RR to carbonaceous products over catalysts.

2.2. Performance Evaluation Metrics of Electrocatalytic CO_2 Reduction Reaction

CO_2RR performance is usually evaluated through FE of products, partial current density, product formation rate, overpotential, energy efficiency (EE) and stability [51–54]. To quantify the products generated during reaction process, gas-phase and liquid-phase products are analyzed using gas chromatography and nuclear magnetic resonance spectroscopy in a corresponding manner. The FE of various reduction products can be quantified via the formula presented below [10]:

$$\mathrm{FE} = (z \times n \times F)/Q \quad (1)$$

In this formula, z stands for the number of transferred electrons, F corresponds to the Faraday constant, n refers to the total moles of the target reduction product formed, and Q refers to the overall charge consumed over the electrolysis process. The FE data quantifies the selectivity of CO_2RR catalysts toward various reduction product. Combined with the market prospect and economic benefit of various carbon-containing compounds, electrolysis systems with elevated C_{2+} FE possess greater application potential. As a widely accepted standard, a C_{2+} FE over 80% serves as the baseline to realize industrialized CO_2RR application [55]. Additionally, exclusive generation of a single gas or liquid product brings distinct advantages, since such a reaction outcome omits subsequent separation procedures and decreases industrial expenditure.

Apart from selectivity metrics, the partial current density of a target product quantifies the actual product formation rate, and together with the production rate, directly reflects practical productivity. In addition, overpotential is defined as the potential difference between the applied potential and the equilibrium potential. It represents the thermodynamic penalty of the reaction and should be minimized to reduce electrical energy input. EE couples the operating cell voltage with the FE of the target product, constituting the most meaningful descriptor for the energy cost of industrial CO_2RR. Finally, long-term operational stability acts as an essential criterion to judge the comprehensive property of catalysts and electrolytic reactors toward CO_2RR [56–60]. This imposes stringent demands on both the structural robustness of catalysts and the operational reliability of electrolytic reactors [61,62]. The long-term operational stability is commonly assessed via long-time performance tracking under constant applied potential or galvanostatic conditions. Industrial electrocatalytic systems intended for mass

manufacturing demand steady operation lasting several thousand hours [63]. Unfortunately, most existing catalysts fail to satisfy such rigorous stability standards, and further targeted research is urgently needed to achieve substantial advancements in this field. Beyond selectivity and stability discussed above, the working current density delivered by catalytic electrodes constitutes another indispensable evaluation metrics. A current density of 200 mA cm^{-2} is widely acknowledged as the minimum benchmark for viable commercial demand of CO_2RR [64,65]. Reactors commonly adopted in current studies include flow cells and H-type cells. The H-type cells consist of a cathode chamber and an anode chamber. During the reaction, CO_2 diffuses to the surface of the working electrode through gas channel. Nevertheless, limited by the low solubility of CO_2, the reaction suffers from severe mass-transport constraints, which results in relatively low reaction currents. In contrast, flow cells employ gas diffusion electrodes with separate channels for electrolyte and gas, enabling well-constructed triple-phase interfaces and thereby substantially boosting the reaction current. To achieve high-efficiency electrocatalytic CO_2 conversion in future research, substantial efforts are still required to design catalysts and reaction devices that simultaneously deliver outstanding performance across all the above evaluation metrics.

3. Intrinsic Structural Modulation of MOF for Electrocatalytic CO_2 Reduction Reaction

As elaborated in the foregoing section, many research efforts have been dedicated to the modulation of MOF-based catalysts to advance high-efficiency CO_2RR performance. This section summarizes existing intrinsic structural modulation strategies of MOF toward CO_2RR, which presents representative catalytic performance and instructive structure-activity relationships. Here, this review will expand on the discussion of structural regulation strategies from modulation of metal nodes and ligand engineering.

3.1. Modulation of Metal Nodes

MOF materials possess structurally designable metal nodes and organic linkers, rendering them suitable for the rational design of catalysts. In general, the reduction products derived from distinct metal sites in conventional catalysts follow inherent regularities. Accordingly, such strategies can be referenced to guide the fabrication of MOF-based catalysts during their performance modulation.

As one of the rare metallic catalytic sites capable of yielding C_{2+} products during CO_2RR, Cu has garnered widespread research interest in the design of MOF-based CO_2RR catalysts [66–70]. For instance, Hinogami and co-workers reported the synthesis of Cu rubeanate MOF and investigated its catalytic performance towards CO_2RR in 2012 [71]. This catalyst successfully reduced CO_2 into HCOOH, which validated the enormous potential of MOF in CO_2RR. In the same year, Kulandainathan et al. investigated the CO_2RR performance of HKUST-1 in organic electrolyte, in which oxalic acid was generated through the dimerization pathway of Cu(I)-CO_2 intermediates [72]. Although both of the above studies focus on Cu-based MOF catalysts, they deliver distinctly different product selectivity, which is primarily attributed to the differences in catalyst coordination environments and electrolysis conditions. Maximizing the proportion of C_{2+} products is essential to promote the practical application of such electrocatalysts for CO_2RR. Apart from monocopper metallic nodes, cluster-type Cu active centers have also been exploited to fabricate electrocatalytic MOF toward CO_2RR. Dong and coworkers engineered a hexanuclear Cu cluster with prominent cuprophilic bonding interactions to assemble robust NNU-50 MOF material [73]. This catalyst delivered a CH_4 FE reaching 66.4% alongside outstanding operational durability for CO_2RR. Furthermore, experimental investigations revealed that the composition and morphology of NNU-50 MOF exhibit no obvious changes before and after the test, demonstrating that the MOF framework can be well maintained during catalysis and further confirming its outstanding stability.

Tuning metal nodes to Zn for the design of MOF catalysts has also attracted considerable attention in CO_2RR research. Benefiting from large specific surface area, homogeneous pore channels and robust metal-ligand coordination bonds, zeolitic imidazolate frameworks (ZIF) were initially adopted for CO_2RR by Wang and co-workers [74]. Three varieties of ZIF-8 nanostructures derived from distinct zinc raw materials were synthesized and evaluated for converting CO_2 into CO. Han and co-workers utilized a mixed solvent composed of 75% 1-dodecyl-3-methylimidazolium chloride and 25% glycerol to synthesize various Zn-1,3,5-benzenetricarboxylic acid (Zn-BTC) MOF by tuning the dosage of zinc chloride, and their CO_2RR performances were evaluated in ionic liquid electrolyte [75]. Experimental results demonstrated that the sheet-like Zn-MOF fabricated under optimal conditions delivered outstanding catalytic performance and stability with a FE of CH_4 up to 88.3%. This work realized the synthesis of diverse MOF materials by modulating the dosage of zinc chloride, which effectively tuned the product selectivity toward CO_2RR. This demonstrated that the regulation of metal nodes was a valid and efficient strategy to optimize the catalytic performance of MOF electrocatalysts. Furthermore, HCOOH is also one of the dominant products generated over Zn-based MOF catalysts during CO_2RR. Zhan and coworkers developed

a Zn-centered MOF named FJU-126-4F, whose microenvironment around active sites was modulated through ligand substitution (Figure 2A) [76]. Similarly, powder X-ray diffraction and infrared spectroscopy confirmed that the MOF structure remains unchanged during the reaction, verifying that the MOF serves as the catalytic active site for the CO_2RR process. Electrochemical measurements carried out in an H-cell demonstrated that this catalyst delivered a FE_{HCOOH} of 60.5% alongside a partial current density of 19.4 mA cm^{-2} at −1.47 V vs. reversible hydrogen electrode (RHE). The catalytic performance originated from the electron-withdrawing tetrafluorinated ligand, which stabilized adsorbed *OCHO intermediates adjacent to Zn-O/N catalytic centers and accelerated CO_2 activation through Lewis acid-base interactions. *In-situ* electrochemical impedance spectroscopy characterization and turnover frequency calculations collectively verified that the FJU-126-4F possessed accelerated charge transport kinetics and superior intrinsic catalytic activity. Although the catalytic mechanism of this catalyst has been well elucidated, improving its operational current density is critical for advancing its practical application in CO_2RR.

Tuning metal nodes to Bi, Ti, and In can also boost the HCOOH selectivity of the products, since these metals tend to anchor CO_2 through oxygen bonding interaction [77]. Particularly, Bi draws extensive research interest for CO_2RR due to its natural abundance and suppressed hydrogen evolution reaction. For example, Zhang et al. adopted BTC linker together with DMF solvent to fabricate Bi-MOF via a hydrothermal bottom-up route and examined its catalytic performance for CO_2RR [78]. Additionally, Sun and co-workers developed a two-dimensional porous Bi-based MOF catalyst with outstanding stability [79]. This catalyst elevated HCOOH selectivity during 30 h continuous electrolysis, delivering a maximum FE of 92.2%. The investigation results indicated that the boosted activity originates from the greater CO_2 uptake capacity and reduced interfacial charge transfer resistance of Bi-MOF.

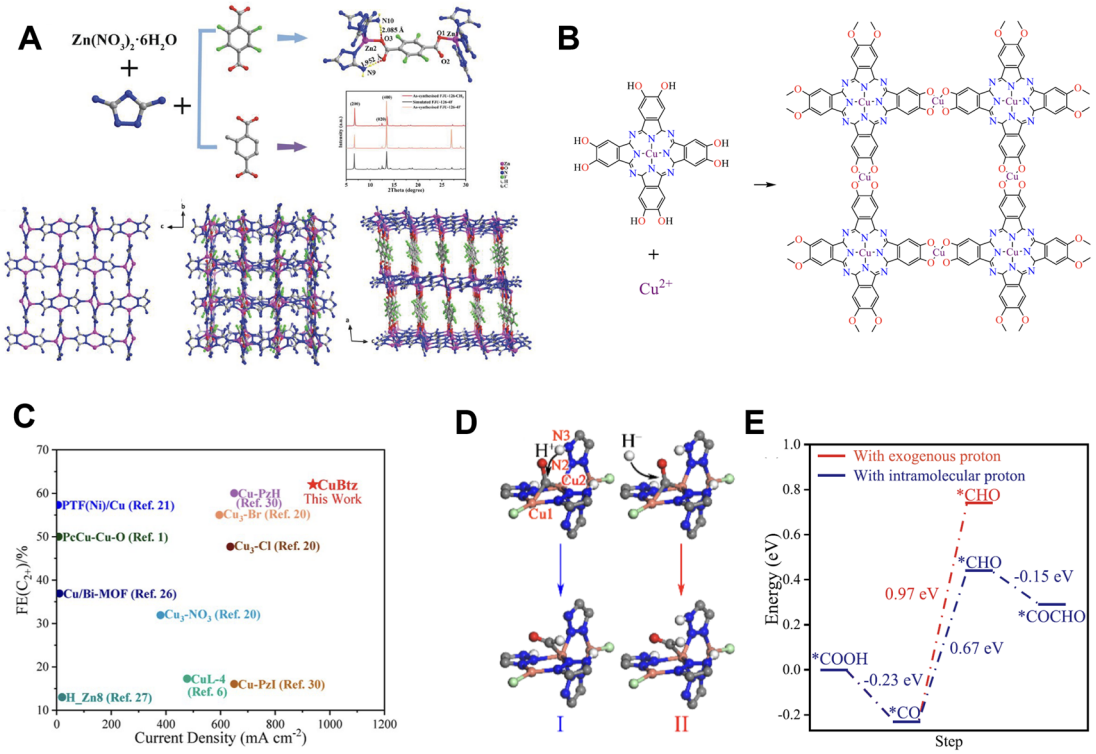

Figure 2. (**A**) Synthesis and structural illustrations of FJU-126-4F, where [Zn_2(DATR)$_2$] units assemble into a 2D layer, further constructing a BDC-4F-pillared 3D open framework. Reproduced with permission from ref. [76]. Copyright 2024, Wiley. (**B**) Structure illustrations of PcCu-Cu-O. Reproduced with permission from ref. [80]. Copyright 2021, American Chemical Society. (**C**) Comparison of CO_2RR performance of CuBtz with other catalysts. (**D**) Possible routes for the hydrogenation of *CO to *CHO on CuBtz. (**E**) Gibbs free-energy barriers of CO_2RR steps. Reproduced with permission from ref. [81]. Copyright 2022, American Chemical Society.

Although such MOF exhibit outstanding electrocatalytic performance, it is evident that C_1 chemicals dominate the products of CO_2RR catalyzed by MOF, while the yield of high-value C_{2+} products remains relatively low. To enhance the selective toward C_{2+} products, Liao et al. prepared two-dimensional MOF denoted as PcCu-Cu-O (Figure 2B) [80]. Benefiting from robust interlayer π-π stacking interactions and high crystallinity of PcCu-Cu-O, the as-prepared MOF realized prominent C_2H_4 selectivity with a FE of 50%. Importantly, powder X-ray

diffraction, X-ray photoelectron spectroscopy, and *in-situ* operando X-ray absorption spectroscopy were employed to identify the catalytic centers. The results revealed that PcCu-Cu-O remained intact under reductive conditions, thereby playing a critical role in CO_2RR. A synergistic catalytic mechanism with dual Cu active sites was accordingly proposed to explain the high efficiency of C-C bond formation, in which CO intermediates generated at CuO_4 sites readily migrate and couple with pre-adsorbed *CO species anchored on adjacent CuPc units. Similarly, with modulation centered on metal nodes, Zhu and coworkers also pointed out that isolated Cu sites possess inherent structural defects [81]. Such defects severely hindered the efficient intermolecular C-C coupling reaction and constituted the primary reason for poor selectivity toward C_{2+} products. To tackle this bottleneck, they synthesized CuBtz MOF, in which the Btz^- ligand coordinates two Cu(I) ions to form binuclear Cu(I) configurations, while its aromatic rings generate intermolecular π-π stacking interactions that stabilize the framework. As shown in Figure 2C, electrochemical measurements revealed that this catalyst achieved a maximum C_{2+} FE of 61.6% with a current density up to 1 A cm^{-2}. Density functional theory (DFT) results revealed that the *CO intermediate bridging two Cu atoms exhibits a more favorable pathway for C-C coupling (Figure 2D,E). Accordingly, the modulation of bimetallic nodes accelerates reaction kinetics and optimizes the CO_2 adsorption energy of catalysts, thereby enabling the production of C_{2+} products. The above cases demonstrate that tuning metal nodes can regulate the product distribution of CO_2 reduction, which represents one of the most extensively investigated modulation strategies to date.

3.2. Ligand Engineering

Organic linkers within MOF not only serve as far more than rigid structural skeletons that support the overall crystalline framework but also function as catalytically active components that regulate the CO_2RR performance through various synergistic mechanisms [82,83]. The introduction of electron-donating or electron-withdrawing substituent onto organic ligand backbones offers a straightforward strategy to precisely adjust the electron density distribution centered at metal active nodes, which further modulates the binding affinity of reaction intermediates on catalytic sites. Beyond electronic regulation, tailored functional groups grafted onto linkers can simultaneously boost the intrinsic CO_2 capture capacity and electrical conductivity of MOF materials.

Electron-abundant catalytic sites are widely acknowledged to facilitate CO_2 activation behavior, as such sites can deliver more electrons toward the anti-bonding orbitals of CO_2 molecules to trigger molecular activation [84]. Guided by this principle, Dou and co-workers implemented a post-synthetic modification strategy to implant highly electron-donating 1,10-phenanthroline units into the ZIF-8 lattice. This modification greatly accelerated charge migration, so the catalyst presented superior electrocatalytic activity compared to unmodified ZIF-8 [85]. This study demonstrated that tuning the electronic properties of ligands can effectively boost the reaction kinetics of CO_2RR. In addition, functionalized ligand groups can construct efficient electron transmission channels within MOF lattices, thereby optimizing the electrical conductivity of the framework [86,87]. As shown in Figure 3A, Yi et al. utilized NiPc as a structural precursor to fabricate phthalocyanine-based NiPc-NiO_4 MOF via a conventional solvothermal route [88]. The bulk MOF powder was further exfoliated into ultrathin 2D nanosheets through high-frequency ultrasonic treatment. This modified catalyst exhibited favorable electrical conductivity, which enables fast electron transport toward catalytic active sites during CO_2RR and thereby enhances electrochemical performance and energy conversion efficiency. CO_2RR measurements revealed that NiPc-NiO nanosheets achieve a FE_{CO} of 98.4% at −0.85 V vs. RHE, which is considerably higher than that of pristine NiPc-OH. DFT results indicated that electron-rich NiPc centers interact more strongly with CO_2 molecules, rendering such sites the dominant catalytic active centers during the reaction (Figure 3B). This work achieved an ultrahigh CO selectivity and demonstrated great application potential for CO_2RR. Meanwhile, this finding validated the feasibility of optimizing CO_2RR performance via rational ligand regulation.

Ligand modification strategies can also regulate the local coordination microenvironment of metal active centers. For instance, Huang et al. synthesized the OH^- functionalized Co-based MOF material (NNU-15) and explored its CO_2RR performance [89]. The hydroxide ligands bound to cobalt centers, a structural feature that conferred the material with robust CO_2 uptake capacity and outstanding electrocatalytic conversion activity. Electrochemical tests revealed that NNU-15 achieved a maximum FE_{CO} of 99.2% at −0.6 V vs. RHE, along with ultra-long catalytic stability up to 110 h. The characterization confirmed the synergistic interaction between Co active sites and coordinated OH^- facilitated efficient CO_2 capture and activation, which promoted the generation of the vital HCO_3^- intermediate. In another work, Jiang et al. explored the CO_2RR performance of a series of sodalite-type ZIFs with varied imidazolate linkers [90]. Their results verified that imidazolate ligands coordinated with Zn(II) centers serve as catalytic active sites for CO_2 conversion, which dominate the catalytic performance. ZIF-8 outperformed other ZIF counterparts by balancing the generation of key *COOH intermediate and

suppression of competitive hydrogen evolution reaction, delivering a peak FE_{CO} of 81%. This work achieved ligand modulation on catalysts of the identical category and visually clarified how ligand design governs the product selectivity of catalysts. Additionally, Al-attas et al. adopted a ligand engineering strategy to optimize the CO_2RR performance of Zn-based MOF catalysts [91]. Two types of Zn-MOF with distinct ligand structures were synthesized for comparative experiments, including $Zn_2(Tz)_2O_x$ (CALF20) constructed by Zn ions and 1,2,4-triazolate ligands, and $Zn(MeIm)_2$ (ZIF-8) assembled from Zn centers and 2-methylimidazolate ligand (Figure 3C,D). Electrochemical test results indicated that CALF20 exhibits superior CO selectivity compared with ZIF-8, with the optimal CO partial current density of −32.8 mA cm^{-2} obtained at −0.97 V vs. RHE. X-ray spectroscopic measurements and DFT verified that ligand regulation dramatically altered the electronic states of Zn centers and facilitated charge transfer in CALF20. This process boosted the generation of *COOH intermediates, endowing the catalyst with outstanding CO partial current density and selectivity.

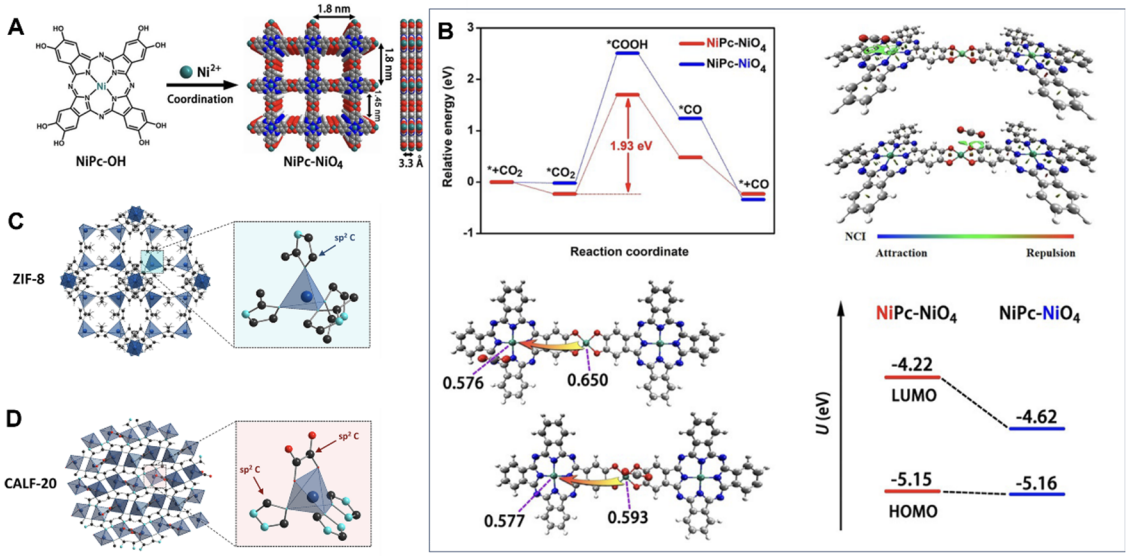

Figure 3. (**A**) Schematic illustration for the preparation of $NiPc-NiO_4$. (**B**) Calculated energy diagrams, Mulliken charges, noncovalent interaction and HOMO/LUMO energy levels of various Ni atoms in $NiPc-NiO_4$. Reproduced with permission from ref. [88]. Copyright 2021, Wiley. (**C**,**D**) Schematic illustrations of the crystal structures of ZIF-8 and CALF20, together with the chemical structures of polyhedral zinc nodes. Reproduced with permission from ref. [91]. Copyright 2021, American Chemical Society.

Modifying ligands with electron-donating or electron-withdrawing substituents efficiently tunes the electron density of metal sites and the adsorption strength of reaction intermediates. Meanwhile, functional groups grafted on linkers improve CO_2 uptake and material conductivity, while constructing coordination environments around metals to stabilize intermediates and reduce the reaction energy barrier. All these highlight ligand engineering as a flexible approach to optimize MOF electrocatalytic activity toward CO_2RR.

4. Construction of MOF-Based Composite Materials for Electrocatalytic CO_2 Reduction Reaction

Composite construction that integrates MOF with various complementary functional components primarily addresses the intrinsic drawbacks of pristine MOFs, which severely impede the efficiency of the CO_2RR process. Meanwhile, the heterointerfaces formed between MOF and other functional units can generate unique synergistic catalytic effects. Such interfacial cooperation can modulate the electronic configuration of metal active centers, optimize the adsorption/desorption strength of key intermediates, and even accelerate the overall reaction kinetics, thereby elevating the catalytic performance of MOF electrocatalysts.

4.1. MOF/Metal Material Composites

Fabrication of MOF/metal nanoparticle composites mainly relies on noble and non-noble metals for modulation. Both types possess distinct intrinsic advantages, and have attracted extensive research interest in CO_2RR. As a typical non-noble metal catalytic material, Cu has been widely integrated with MOF through many synthesis strategies [92–95]. In a representative study in 2017, Hupp and co-workers developed a facile synthetic route to immobilize Cu NPs within the hexagonal pore channels of NU-1000 (Figure 4A) [96]. The team first

introduced single-site Cu(II) species into NU-1000 thin films through solvothermal deposition, followed by electrochemical reduction to convert Cu(II) species into metallic Cu active nanoparticles. Such composite structural design increased the number of exposed active sites during catalytic process, and thus realized a formate FE of 28% under same reaction conditions. In addition, boosting the selectivity toward C_{2+} products has attracted considerable research attention within this strategy. The rational integration of Cu species with MOF represents a highly promising modification strategy for designing CO_2RR catalysts with enhanced C_{2+} products selectivity. Inspired by such modulation strategies, Nam et al. reported an interesting electrode design for efficient CO_2RR [97]. In their work, HKUST-1 MOF was first immobilized on the polytetrafluoroethylene substrate, followed by the deposition of a 300 nm-thick Cu layer to construct the hierarchical electrode (Figure 4B). When evaluated in a flow cell configuration, the as-fabricated catalyst delivered a maximum FE of 51% for C_2H_4 with a high partial current density of 491 mA cm^{-2}. Mechanistic investigations revealed that the remarkable electrocatalytic performance benefited from the intrinsic CO_2 enrichment capability of HKUST-1. Meanwhile, the generated Cu-Cu active sites effectively promoted *CO dimerization, which substantially facilitated the production of C_2H_4.

Beyond non-noble metal-based composites, the composite construction of noble metal and MOF also exhibit high-performance CO_2RR activity. To realize efficient C_{2+} products generation, Xie and coworkers successfully anchored Au nanoneedles within PCN-222 frameworks with isolated Cu porphyrin active sites, constructing a novel AuNN@PCN-222(Cu) hybrid electrocatalyst (Figure 4C) [98]. Electrochemical tests revealed that this composite catalyst achieved a FE of 52% toward C_2H_4 at −1.2 V vs. RHE. Further experimental explorations showed that the excellent C_2H_4 production performance originated from the bimetallic synergistic effect between Au nanoneedles and Cu-based MOF. In the catalytic process, the construction of composite catalysts enables cascade optimization of the catalytic pathway and thereby facilitates the production of high-value products. As presented in Figure 4D, Mukhopadhyay et al. also constructed a MOF-Ag heterostructure by *in-situ* growing UiO-66 thin films on bulk Ag substrates to tailor the microenvironment of Ag active sites [99]. Experimental observations revealed that the MOF layer optimized the mass transfer of reactants, thereby increasing the local CO_2 concentration around Ag active sites. Meanwhile, the Brønsted acidic groups derived from UiO-66 stabilized the key $*COO^-$ intermediate, which ultimately facilitated the generation of CO. Moreover, the construction of such composite structure suppressed the competitive hydrogen evolution reaction, achieving a high CO selectivity of 89%.

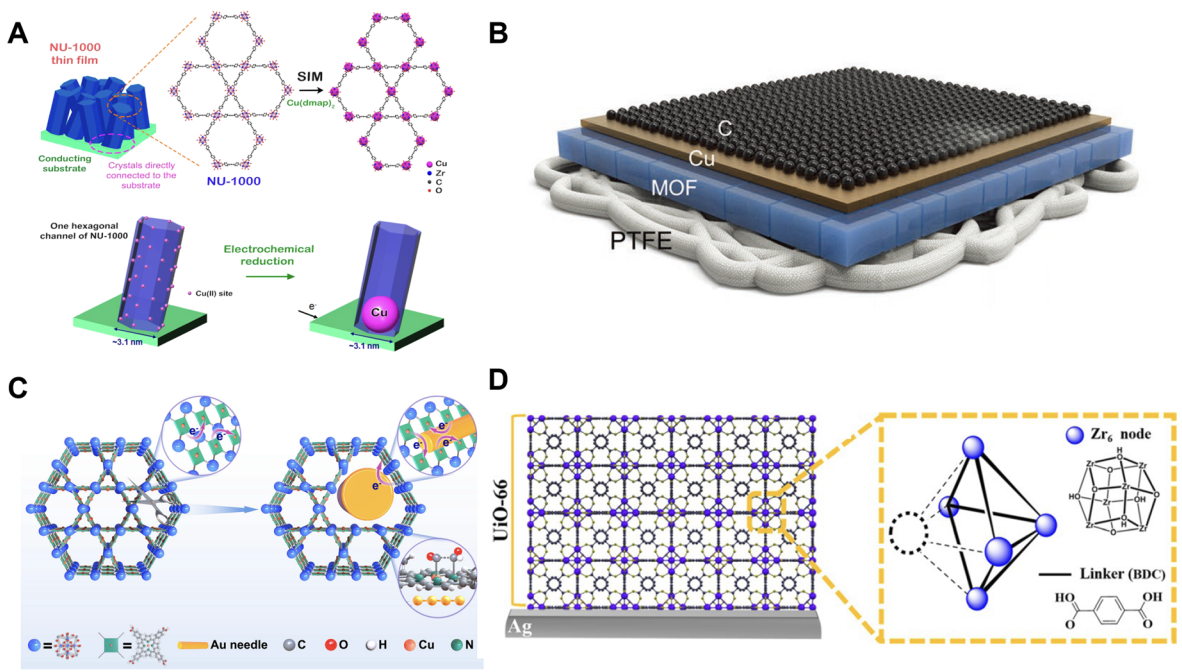

Figure 4. (**A**) Schematic representation of Cu NPs within the hexagonal pore channels of NU-1000. Reproduced with permission from ref. [96]. Copyright 2017, American Chemical Society. (**B**) Schematic of MOF-augmented gas diffusion electrode components. Reproduced with permission from ref. [97]. Copyright 2022, Wiley. (**C**) Schematic representation of impregnation of Au nanoneedles into PCN-222(Cu). Reproduced with permission from ref. [98]. Copyright 2022, Springer Nature. (**D**) Illustration of the structure of a UiO-66 thin film assembled on an Ag electrocatalyst and missing-cluster defect in UiO-66. Reproduced with permission from ref. [99]. Copyright 2021, Wiley.

This section has presented the fabrication strategies of MOF/metal material composites for CO_2RR. The combination of MOF with functional metal species effectively modulates the electronic microenvironment and increases the number of accessible active sites, thereby improving electrocatalytic performance. Fabricating MOF/metal composite catalysts provides a reliable strategy for designing high-performance electrocatalysts toward CO_2RR. Nevertheless, precise modification of metal active sites should be prioritized in follow-up investigations to guarantee stable catalytic performance and enable an accurate understanding of catalytic mechanisms.

4.2. MOF/Metal Oxide Material Composites

Compositing metal oxide with MOF can simultaneously inherit the advantages of frameworks while integrating the catalytic properties of metal oxide. Benefiting from the catalytic active sites and unique electronic environments generated by such hybridization, the resultant catalysts generally exhibit outstanding catalytic activity. Accordingly, this strategy has attracted extensive attention as a modulation strategy in the design of MOF-based catalysts.

To boost C-C coupling and facilitate the production of C_{2+} products, Zhang et al. fabricated Cu_2O-embedded NiCu bimetallic MOF nanorod arrays grown on Cu foam substrates (Cu_2O@NiCu-MOF/CF), wherein the heterostructure promotes effective interfacial charge modulation [100]. Figure 5A revealed that introduced Ni shortens the bonding distance between metal sites and adsorbed *CO species, substantially strengthening the affinity toward *CO intermediates. This improved local *CO concentration surrounding Cu sites and accelerated the dimerization of *CO-*COH. As presented in the reaction paths, the charge accumulation on Ni sites offered superior stabilization for the $*OCHCH_3$ intermediate, thermodynamically favoring CH_3CH_2OH formation (Figure 5B). The construction of MOF/metal oxide hybrids can not only regulate the electronic environment, but also suppress catalyst agglomeration via interfacial effects. Therefore, this structural advantage expands the specific surface area, maximizes the exposure of active sites, and ultimately enhances electrocatalytic activity. Via a single hydrothermal conversion treatment of ZIF-7 within silver nitrate solution, Bao and coworkers synthesized a layered ZIF matrix decorated with Ag_2O nanoparticles [101]. Loaded Ag_2O nanoparticles successfully suppressed the self-aggregation of ZIF, which enlarged the surface area and exposed abundant accessible Ag catalytic sites. Benefiting from the interfacial synergy between Ag_2O nanoparticles and ZIF-7, this hybrid catalyst presented a FE of 80% for CO production, outperforming bare ZIF-7 and Ag-carbon composite catalysts. Collectively, the above examples demonstrate that the integration of MOFs with metal oxides generates prominent interfacial effects and facilitates the exposure of active sites, which fundamentally accounts for the enhanced catalytic activity of composite catalysts.

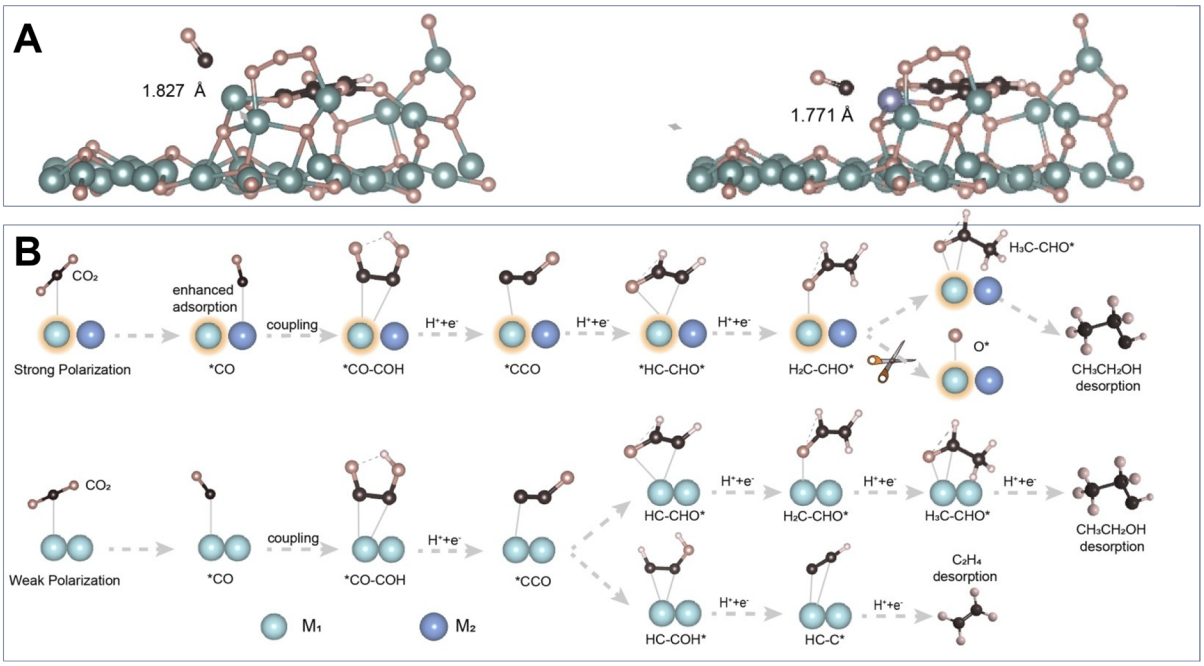

Figure 5. (**A**) Schematic representation of the adsorption of *CO and (**B**) The various CO_2RR path over Cu_2O@Cu-MOF/CF and Cu_2O@NiCu-MOF/CF. (**C**) synthesis for Ag_2O/layered ZIF. Reproduced with permission from ref. [100]. Copyright 2023, Wiley.

5. Design of MOF-Derived Materials for Electrocatalytic CO_2 Reduction Reaction

As discussed in the preceding section, intrinsic MOF electrocatalysts suffer from the poor intrinsic electrical conductivity and inferior structural stability under harsh conditions [102–104]. Even though node/ligand modification and composite engineering can alleviate these issues to a certain extent, most pristine MOF still undergo framework collapse or rapid active site deactivation during long-term CO_2RR process. In contrast, transforming MOF precursors into functional derivatives via high-temperature pyrolysis or *in-situ* electrochemical reconstruction provides a promising strategy to simultaneously retain the inherited high porosity, uniform metal dispersion and tunable topological advantages of MOF, while drastically boosting electron transport capability and electrochemical durability [105–107]. This section summarizes the relevant design strategies of catalysts from two primary categories, which include MOF-derived single-atom catalysts and MOF-derived metal/metal oxide catalysts.

5.1. MOF-Derived Single-Atom Catalysts

Single-atom catalysts consist of isolated metal atoms atomically anchored onto heteroatom-doped carbon substrates, which represent the theoretical limit of metal atom utilization efficiency and have attracted extensive research attention in numerous fields such as CO_2RR in recent years [108–110]. MOF feature periodically distributed metal nodes uniformly confined within organic ligand skeletons, which can effectively suppress metal agglomeration during high-temperature carbonization. Hence, considerable attempts have been made to establish synthetic strategies for high-performance catalysts relying on MOF pyrolysis treatment [111,112]. After pyrolysis, the organic linkers carbonize into N-rich porous carbon carriers, while isolated metal atoms are immobilized via M-N_x coordination bonds to avoid sintering and particle growth. Compared with nanoparticle catalysts, MOF-derived SACs exhibit unique electronic structures and optimized intermediate adsorption energies, thus simultaneously enhancing CO_2RR activity and target product selectivity. At present, the synthetic routes reported in existing studies fall into two categories, namely direct pyrolysis of monometallic/bimetallic MOF precursors and heteroatom-assisted pyrolysis.

5.1.1. Derived Single-Atom Catalysts

As shown in Figure 6A, Zhang et al. reported the synthesis of Bi single atoms supported on N-doped carbon (Bi SAs/NC) via calcining a physical mixture of Bi-MOF and dicyandiamide at 600 °C under Ar condition [113]. Aberration-corrected high-angle annular dark-field scanning transmission electron microscopy and X-ray absorption near-edge structure characterizations confirmed the existence of Bi single atoms as well as the exclusive Bi-N_4 coordination configuration generated after pyrolysis. DFT calculations demonstrated that the Gibbs free energy barrier for *CO_2 protonation to *COOH over Bi-N_4 sites was markedly lower than Bi nanoparticles or Bi clusters composites. As a result, Bi SAs/NC delivered a maximum FE of 97% for CO at −0.5 V vs. RHE, outperforming other Bi-based catalysts. This work delivers excellent CO selectivity, which greatly promotes the practical prospects of CO_2RR and further verifies the rationality and feasibility of the proposed catalyst design strategy. Besides, structural engineering centered on the M-N_4 structure can also be adopted to further boost catalytic performance. For instance, Chen et al. proposed an amination modification strategy to tune the electronic structure of single-atom catalysts, and synthesized amino-functionalized Ni-N_4/C single-atom materials via a combined hydrothermal-pyrolysis route [114]. In CO_2RR measurements conducted in an H-type electrolytic cell, the CO partial current density of the as-prepared catalyst was 2.5 times higher than that of unmodified Ni-N_4/C. Moreover, when loaded on a gas diffusion electrode and tested in a flow cell, this catalyst delivered an outstanding CO partial current density of 447.6 mA·cm^{-2}, which strongly verifies that amination modification can effectively improve catalytic activity. DFT calculations revealed that amino groups can modulate the electronic distribution of M-N-based carbon catalysts, strengthen the adsorption of reaction intermediates and accelerate interfacial charge transfer, thereby facilitating the activation and reductive conversion of CO_2.

Additionally, tuning the metal sites of MOF precursors enables facile modulation of single-atom catalytic sites, which represents one of the prevalent strategies to regulate product selectivity. Zhao et al. fabricated Cu single-atom nitrogen-doped porous carbon electrocatalysts by pyrolyzing Cu-doped ZIF-8 precursors at 1000 °C under N_2 atmosphere (Figure 6B) [115]. The as-obtained catalysts exhibited electrocatalytic activity toward CO_2 reduction to acetone with a FE of 36.7%. Structural and mechanistic investigations revealed that the Cu-pyrrolic-N_4 coordination configuration realizes a lower energy barrier for CO_2 activation, and simultaneously stabilizes reaction intermediates relevant to acetone formation (Figure 6C). Nevertheless, the generation of C_{2+} products remains a formidable challenge over single-atom Cu sites, as the C-C coupling step occurring on isolated Cu centers requires surmounting a remarkably high energy barrier. On this basis, Chen and co-workers synthesized $Fe_1N_2O_2$ single-atom catalysts by pyrolyzing melamine-modified Fe-doped Zn-MOF-74 at 1000 °C [116]. The coexistence of O

and N coordination atoms modified the d-band center of Fe sites, weakening the binding strength of *CO intermediates. The $Fe_1N_2O_2$ catalyst maintained FE_{CO} above 95% across a broad potential window, with negligible performance decay over 12 h continuous electrolysis, far superior to Fe nanoparticles and pure N-carbon supports.

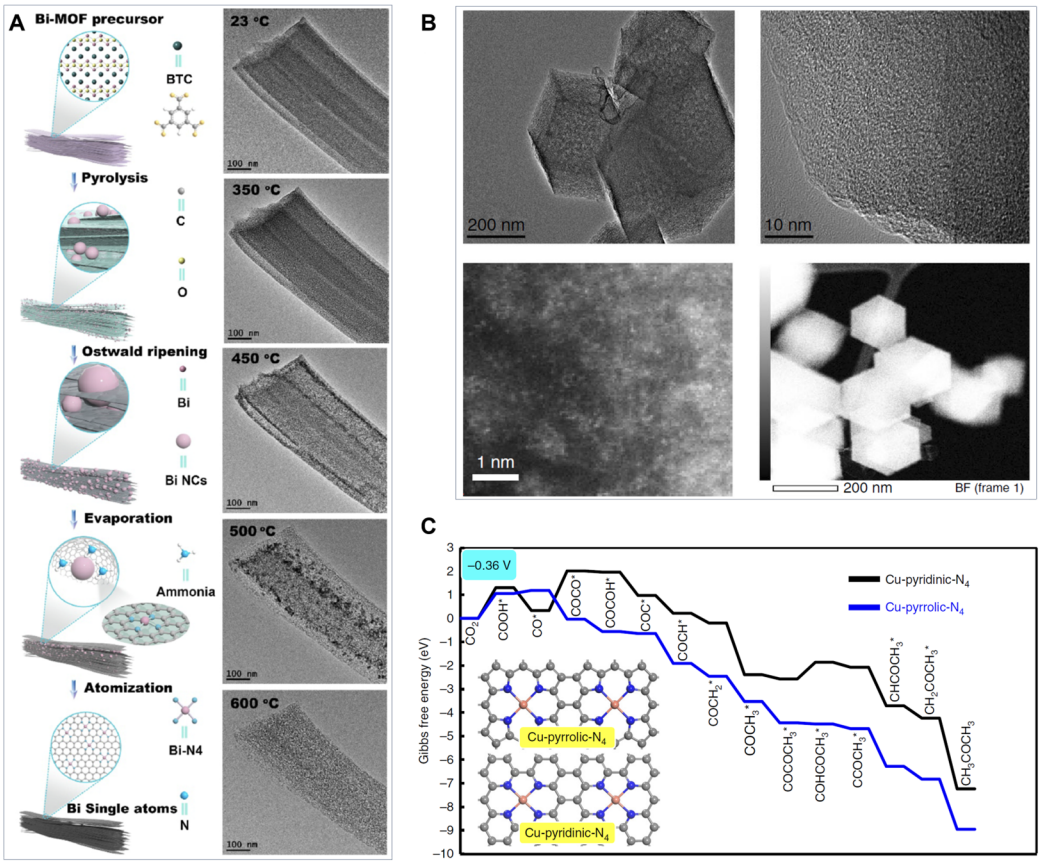

Figure 6. (**A**) Schematic illustration of the transformation process from Bi-MOF to isolated single Bi atoms and the corresponding representative images. Reproduced with permission from ref. [113]. Copyright 2019, American Chemical Society. (**B**) Morphological characterization of Cu single-atom catalyst. (**C**) Free energy diagrams for CO_2RR to acetone at a potential of -0.36 V on Cu-pyridinic-N4 and Cu-pyrrolic-N_4 active sites. Reproduced with permission from ref. [115]. Copyright 2020, Springer Nature.

5.1.2. Derived Dual-Site Single-Atom Catalysts

Introducing a second metal atom into the carbon matrix to construct adjacent dual-atom sites enables electronic modulation of the primary metal center, breaking the single-site scaling limitation and optimizing multi-electron transfer pathways for C_{2+} products generation. ZIF-series MOF with zinc ions as metal nodes represent the most classic precursors for fabricating dual-site single-atom catalysts [117,118]. During pyrolysis, the imidazolate ligands carbonize to construct a porous carbon substrate. Meanwhile, zinc ions within the framework are reduced by carbon to metallic zinc, which is subsequently removed via high-temperature sublimation, generating abundant metal vacancies and nitrogen-doped defect sites. Extraneous metal ions pre-doped at the synthesis stage can be anchored by intrinsic nitrogen heteroatoms in the framework, ultimately forming stable M-N_x single-atom sites. Under this concept, Cu-In dual-atom carbon catalysts (Cu-In-NC) are prepared by pyrolyzing bimetallic ZIF-8 co-doped with Cu^{2+} and In^{3+} precursors (Figure 7A) [119]. During CO_2RR process, Cu served as the core active center for CO_2 activation to *COOH, while In atoms adjusted the electronic density of Cu to reduce the formation free energy of key intermediates. Therefore, Cu-In-NC achieved a FE_{CO} of 96% at −0.7 V vs RHE, with greatly elevated partial current density. Based on the same design strategy, Fe-Ni dual single-atom catalyst derived from Fe/Zn bimetallic ZIF displayed a FE_{CO} of 96.2% at −0.5 V vs RHE, benefiting from the complementary electronic effect between Fe and Ni sites that simultaneously lowered the barriers for CO_2 activation and CO desorption (Figure 7B) [120].

Beyond CO-selective dual sites, Cu-based bimetallic single-atom catalysts hold promise for C_{2+} products, as the catalytic sites provide sufficient positions for *CO dimerization. As presented in Figure 7C, Zheng and co-workers fabricated Cu-Cu dual single-atom catalysts using Cu-MOF as the precursor, and further realized the

utilization of CO_2 via electrocatalytic CO reduction reaction [121]. Electrochemical tests revealed that Cu-Cu atomic sites can immobilize two CO intermediates and facilitate their dimerization process, realizing a C_{2+} FE up to 91% at −1.6 V vs. RHE. Once a Ni atom replaces one Cu site within the bimetallic configuration, the catalyst predominantly produced CH_4, which was attributed to the overly strong binding strength between Ni and *CO intermediates. DFT results revealed that the energy barrier for generating C_{2+} intermediates over Cu-Cu dual sites is lower than that on Cu-Ni dual sites, thereby boosting the production of C_{2+} products.

From a mechanistic perspective, stabilizing one intermediate on isolated single-atom sites typically occurs at the cost of destabilizing others, which renders simultaneous optimization of CO_2 activation, CO desorption, and C-C coupling challenging. In dual-site single-atom catalysts, the two adjacent metal centers feature distinct d-band centers governed by their intrinsic electronic configurations and coordination environments [122]. Direct metal-metal orbital hybridization renormalizes the d-states near the Fermi level and triggers directional charge transfer between the two sites, shifting the d-band center of each metal upward or downward relative to its mononuclear analogue [123]. Consequently, one metal site can retain strong adsorption of *COOH to promote CO_2 activation, while the other site displays weakened binding to *CO to facilitate CO desorption, or suitably modulated binding of *CO and *CHO to reduce the energy barrier for generating the key intermediate. This synergistic catalytic mechanism of dual-site effectively constructs a favorable electronic environment, offering a rational strategy to tune product selectivity toward C_{2+} products.

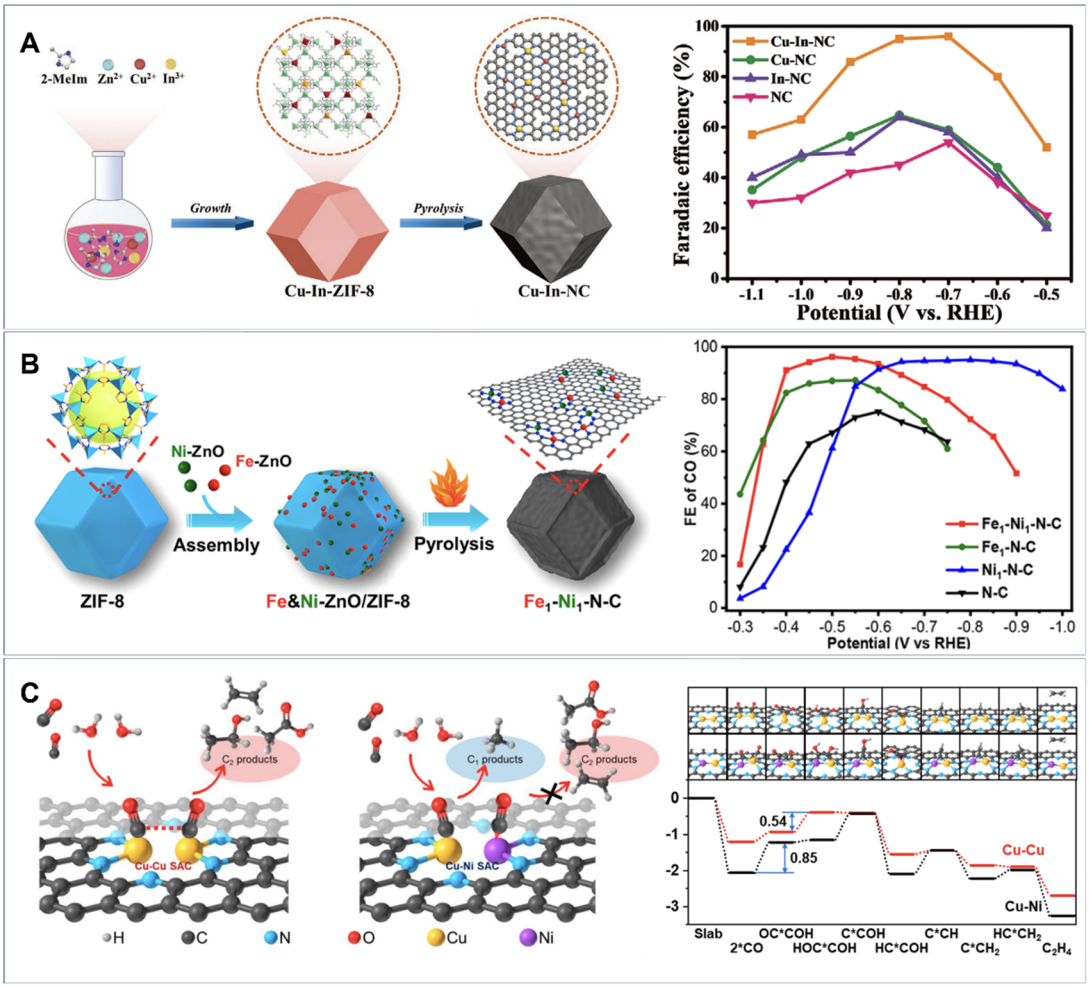

Figure 7. (**A**) Schematic illustration of the synthetic process for Cu-In-NC and the FE of CO. Reproduced with permission from ref. [119]. Copyright 2022, Wiley. (**B**) Schematic illustration of the synthetic process for Fe-Ni dual single-atom catalyst and the FE of CO. Reproduced with permission from ref. [120]. Copyright 2021, American Chemical Society. (**C**) Schematic illustration of reaction and Gibbs free energy for the C_2H_4 formation pathway on dual Cu-Cu and Cu-Ni catalyst. Reproduced with permission from ref. [121]. Copyright 2021, American Chemical Society.

5.2. MOF-Derived Metal/Metal-Oxide Catalysts

Unlike isolated single atoms, metal/metal oxide catalysts contain multi-metal sites, which are indispensable for realizing C-C coupling to produce C_{2+} products. The parent MOF acts as a template during derivation,

restricting excessive particle growth and aggregation, while the residual porous carbon matrix provides fast electron transport ability and mass transfer pathways. This section discusses the above strategy from the perspective of derivative synthesis routes, including *ex-situ* pyrolysis and *in-situ* electrochemical reconstruction.

5.2.1. *Ex-Situ* Pyrolysis

Zang and coworkers carried out thermal treatment of Cu-BTC precursor at high temperature to synthesize CuO_x@C nanoparticles (Figure 8A) [124]. The CuO_x@C catalysts realized a maximum FE of 82% toward C_{2+} products. The remarkable catalytic performance originates from the carbon layers within the derived catalysts, which effectively boost the adsorption of reaction intermediates on Cu sites and thereby leading to high selectivity toward C_{2+} products. Similarly, Wei and co-workers encapsulated Cu nanoparticles within N-doped carbon frameworks (Cu NPs-NC) by thermally decomposing benzimidazole-functionalized Cu-BTC MOF [125]. Experimental observations verified that abundant pyrrolic N and Cu-N sites strengthened CO_2 capture and accelerated C-C bond formation, realizing FE toward C_{2+} products about 20%. Besides forming carbon shells during calcination, the ligands can also be completely removed to yield oxides with porous structures. For example, Yang and coworkers treated Cu-ASP MOF via air annealing to fabricate porous CuO nanowires [126]. Rich metastable Cu sites originating from the metal oxide offered favorable interfaces for *CO-*CO dimerization, boosting the selectivity toward C_{2+} products.

Beyond Cu-based MOF, MOF with Bi, In, Sn metal sites are also applicable to the above-mentioned synthetic strategy, yet HCOOH serves as their major CO_2RR product. Pyrolysis of Sn-MOF afforded a composite Sn(101)/SnO_2/C catalyst, in which the exposed Sn (101) facets exhibit strong adsorption toward the *OCHO intermediate, enabling an exceptional HCOOH FE of 93.3% [127]. Likewise, Sun et al. reported a high-performance catalyst capable of selectively converting CO_2 into HCOOH [128]. Under this strategy, they constructed In-doped porous carbon immobilized with MoP nanoparticles. In a recent investigation, Deng and co-workers carbonized CAU-17 precursors under Ar and air atmospheres, respectively, to obtain carbon nanorod-supported Bi-based catalysts (Bi@C and Bi_2O_3@C, Figure 8B) [129]. In an H-cell, the Bi_2O_3@C-800 presented a high HCOOH FE of 92% at −0.9 V vs. RHE. Further measurements conducted in a flow cell showed that Bi_2O_3@C-800 retained a HCOOH FE exceeding 93%. Mechanism investigation validated that the crystalline Bi-O phase in Bi_2O_3@C-800 accelerated the reaction kinetics, while the carbon matrix effectively reduced charge transfer resistance and facilitated the generation of key intermediates.

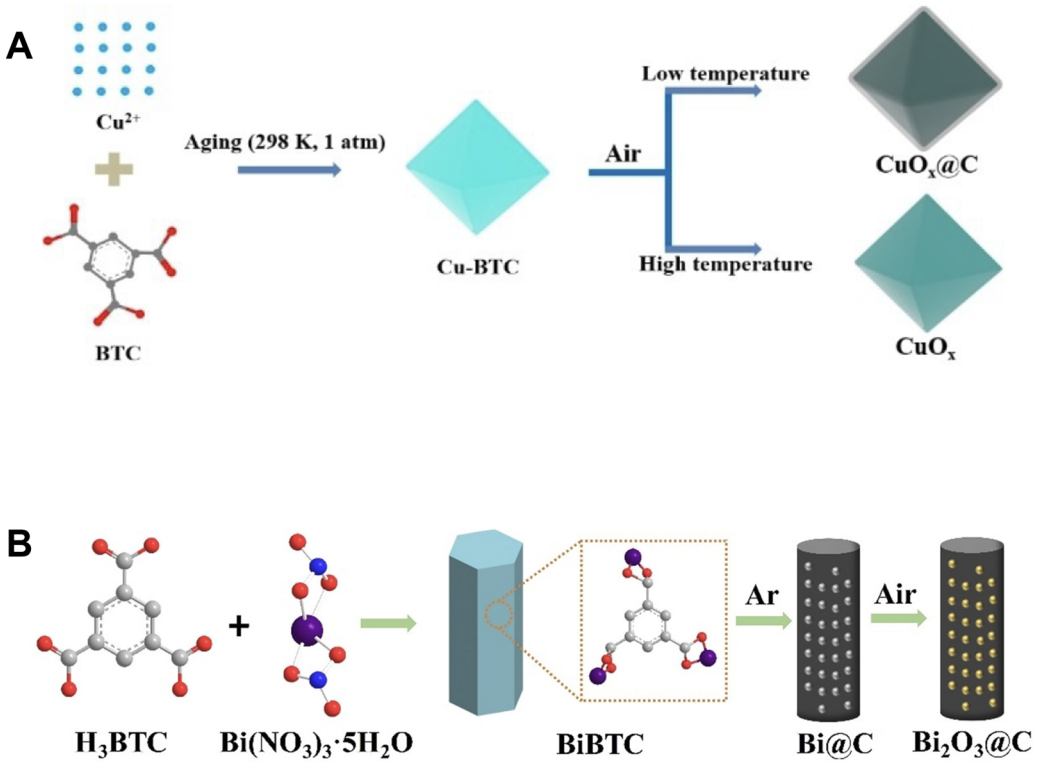

Figure 8. (**A**) Schematic illustration of the synthetic process for CuO_x@C nanoparticles. Reproduced with permission from ref. [124]. Copyright 2022, Wiley. (**B**) The synthesis process of Bi@C and Bi_2O_3@C catalysts. Reproduced with permission from ref. [129]. Copyright 2020, Wiley.

5.2.2. *In-Situ* Electrochemical Reconstruction

Apart from thermal pyrolysis for synthesizing MOF-derived electrocatalysts, *in-situ* electrochemical reconstruction represents another widely adopted fabrication strategy. During this electrochemical transformation, MOF-supported electrodes undergo dramatic structural evolution under reductive potentials, accompanied by breakdown of initial MOF frameworks and formation of metal-based hybrid catalysts derived from intrinsic metal centers of parent MOF. Since these reconstructed catalysts are generated in real-time reductive environments, their exposed active sites are geometrically and electronically optimized for CO_2RR.

Cao and co-workers proposed an electrocatalyst named Cu_2O@CuHHTP, which was fabricated via electrochemical reduction of two-dimensional CuHHTP MOF (Figure 9A) [130]. During the conversion of Cu metal sites into Cu_2O species, abundant uncoordinated hydroxyl groups were generated adjacent to catalytically active sites. These uncoordinated hydroxyl groups were capable of building hydrogen bonding interactions with reaction intermediates, thereby promoting CH_4 generation (Figure 9B). In addition, this synthetic strategy is also applicable to the fabrication of catalysts with high selectivity toward C_{2+} products. As presented in Figure 9C, Huo et al. adopted *in-situ* electrochemical reduction to transform a Cu-MOF constructed with terephthalic acid and 1,4-diazacyclooctane ligands into mesoporous Cu nanoribbons, attaining a FE of 82.3% with a partial current density of 347.9 mA cm^{-2} [131]. Experimental characterizations revealed that the strengthened electric field effect originating from abundant mesopores facilitated the adsorption of K^+ and OH^- at catalytic interfaces, thereby lowering the energy barrier for *CO generation and the following *CO-*CO dimerization toward C_{2+} products.

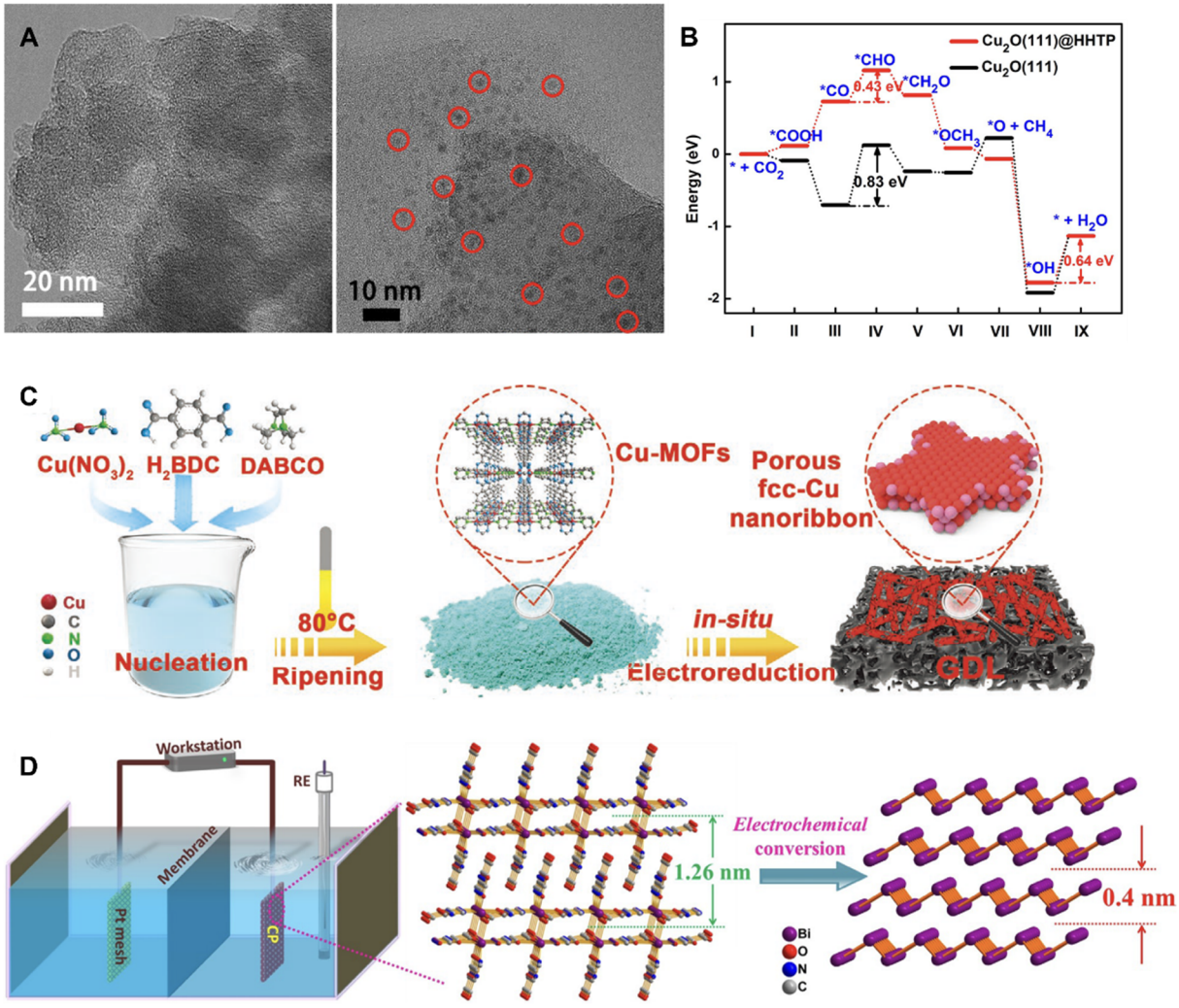

Figure 9. (**A**) Transmission electron microscope images of CuHHTP and Cu_2O@CuHHTP, respectively. (**B**) Gibbs free energy for the CH_4 formation pathway. Reproduced with permission from ref. [130]. Copyright 2020, Wiley. (**C**) The synthesis process of mesoporous Cu nanoribbons. Reproduced with permission from ref. [131]. Copyright 2021, Wiley. (**D**) Schematic illustration for the preparation of Bi-ene. Reproduced with permission from ref. [132]. Copyright 2020, Wiley.

In addition, Bi-based MOFs have also garnered extensive research attention via the *in-situ* electrochemical reconstruction. Cao and coworkers illustrated that ultrathin Bi-containing MOF act as precursor to generate atomic-scale bismuthene (Bi-ene) through *in-situ* electrochemical reconstruction (Figure 9D) [132]. Benefiting from the ultrathin structure with abundant active sites, the Bi-ene catalyst achieved near-unity FE toward HCOOH. Importantly, *in situ* ATR-IR spectroscopy was utilized to monitor key reaction intermediates during the CO_2RR process over Bi-ene catalysts, which provides critical insights into the underlying catalytic mechanism. Another study has recorded the rapid *in-situ* generation of $Bi_2O_2CO_3$ from bismuth-carboxylate MOF under reduction condition [133]. Experimental results revealed that HCO^{3-} can break the coordination bonds between Bi^{3+} and carboxylate groups, stripping off the trimesic acid organic ligands and triggering structural reconstruction of the pristine MOF. The $[Bi_2O_2]^{2+}$generated after reconstruction are identified as the catalytic active sites for CO_2RR. The as-formed $Bi_2O_2CO_3$ nanosheets attain a maximum HCOOH FE of 96.1%, which outperforms most previously reported electrocatalysts. The relevant comparison of catalytic performance is presented in Table 1.

Table 1. A comparison of the CO_2RR performance of relevant catalysts.

Catalysts	Products	FE (%)	E (V vs. RHE)	*j* (mA cm^{-2})	Reactor	Stability (Hours)	Ref.
NNU-50	CH_4	66.4	−1.0	~400	Flow cell	4	[73]
Zn–BTC	CH_4	~88.3	-	~0.5	H-cell	6	[75]
FJU-126-4F	HCOOH	60.5	−1.47	19.4	H-cell	-	[76]
Bi-MOF	HCOOH	92.2	−0.9	41	H-cell	30	[79]
PcCu-Cu-O	C_2H_4	~50	−1.2	7.3	H-cell	4	[80]
NiPc-NiO_4	CO	98.4	−0.85	34.5	H-cell	10	[88]
NNU-15	CO	99.2	−0.6	~5	H-cell	110	[89]
ZIF-8	CO	81	−1.1	~12.8	H-cell	-	[90]
CALF20	CO	94.5	−0.97	32.8	Flow cell	-	[91]
Cu-SIM NU-1000	HCOOH	28	−0.82	-	H-cell	-	[96]
Cu/PTFE	C_2H_4	49	-	−1000	Flow cell	~60	[97]
Cu_2O@MOF/CF	CH_3CH_2OH	44.3	−0.615	~9.7	H-cell	47	[100]
Ag_2O/layered ZIF	CO	80.5	−1.2	26.2	H-cell	-	[101]
$Fe1N_2O_2$/NC	CO	99.7	−0.5	~5	H-cell	12	[116]
Cu-In-NC	CO	96	−0.7	~4	H-cell	~12	[119]
Cu-Cu SAC	C_{2+} products	~91	−1.66	~90	H-cell	-	[121]
CuO_x@C	CH_3CH_2OH	46	−1.0	166	Flow cell	-	[124]
Sn(101)/SnO_2/C	HCOOH	93.3	−0.8	~4	H-cell	13	[127]
Bi_2O_3@C	HCOOH	93	−0.28	200	Flow cell	-	[129]
CuHHTP	CH_4	73	−1.4	10.8	H-cell	-	[130]
Cu nanoribbons	C_{2+} products	82.3	−1.23 V.	347.9	Flow cell	10	[131]
Bi-ene	HCOOH	99.2	-	200	Flow cell	6	[132]
$Bi_2O_2CO_3$	HCOOH	96.1	−0.669	10	H-cell	48	[133]

6. Summary and Outlook

This review systematically summarizes the latest advances in modulation strategies for MOF-based electrocatalysts toward the CO_2RR, covering intrinsic structural regulation of MOF, fabrication of MOF-based composite materials, and design of MOF-derived catalysts. Intrinsic structural modulation, encompassing metal node modulation and ligand engineering, provides molecular-level precision in tuning the electronic structure and coordination microenvironment of active sites, thereby establishing well-defined structure-activity relationships. Composite construction, through the integration of MOF with metal nanoparticles, or metal oxides, effectively compensates for the intrinsic limitations of pristine MOF while introducing synergistic catalytic effects. MOF-derived materials, including single-atom catalyst and metal/metal oxide catalysts, leverage the sacrificial template role of MOF to achieve highly dispersed active sites, offering a versatile platform for enabling C-C coupling toward C_{2+} products. These conclusive results shed light on the targeted construction of advanced MOF catalysts and broaden their application prospects in CO_2RR.

Although the above summary demonstrates that significant advances have been achieved in this field, several aspects still require attention for the development of MOF-based CO_2RR catalysts (Figure 10). First, the dynamic structural evolution of MOF-based catalysts under operando conditions remains insufficiently characterized. Therefore, advanced operando techniques are urgently needed to capture transient reaction intermediates and monitor active-site reconstruction in real time. Second, scalable synthesis of MOF-based catalysts remains a key bottleneck for industrial application, as the crystalline structure and catalytic properties of MOF are highly sensitive to subtle variations in synthesis parameters. Third, the long-term operational durability of MOF-based catalysts under industrially relevant current densities has not yet been subjected to systematic evaluation, and

degradation mechanisms require thorough investigation. For example, high-current electrolysis brings severe interfacial perturbations including local pH change and salt precipitation, which readily destroy MOF structure and accelerate performance decay. Revealing these degradation pathways will facilitate the rational design of robust MOF catalysts, promoting the practical deployment of MOF systems for electrocatalytic CO_2RR. Furthermore, microenvironment modulation of MOF exhibits promising prospects in regulating interfacial reactant distribution, suppressing competing reactions and improving mass transport ability. Nevertheless, precise design of the microenvironment for MOF catalysts remains a considerable challenge. In response to these urgent demands, integrating machine learning with high-throughput computational screening to explore the rational design and modulation of MOF microenvironments holds great potential for discovering high-efficiency catalysts. Meanwhile, bridging lab-scale research and practical industrial deployment requires targeted progress in reactor design. These difficulties mainly lie in modulating the microstructure of catalyst layers and optimizing reaction interfaces. Accordingly, targeted design and upgrades of reaction reactors remain critically important. From an industrial perspective, MOF-based electrocatalysts should be rationally modulated to meet the demands of high current density, long-term stability, and operation with dilute CO_2 streams, which requires the concerted engineering of active sites, pore structures, conductivity and catalytic microenvironments. Specifically, precisely constructed bimetallic or defective sites can maximize intrinsic activity and selectivity. Additionally, hierarchical porosity can accelerate mass transport and enrich local CO_2. Moreover, the construction of conductive MOF can minimize charge-transfer resistance at high current densities. We anticipate that the synergistic modulation of these aspects, combined with advanced reactor design, will enable the practical deployment of MOF-based catalysts in industrial CO_2RR.

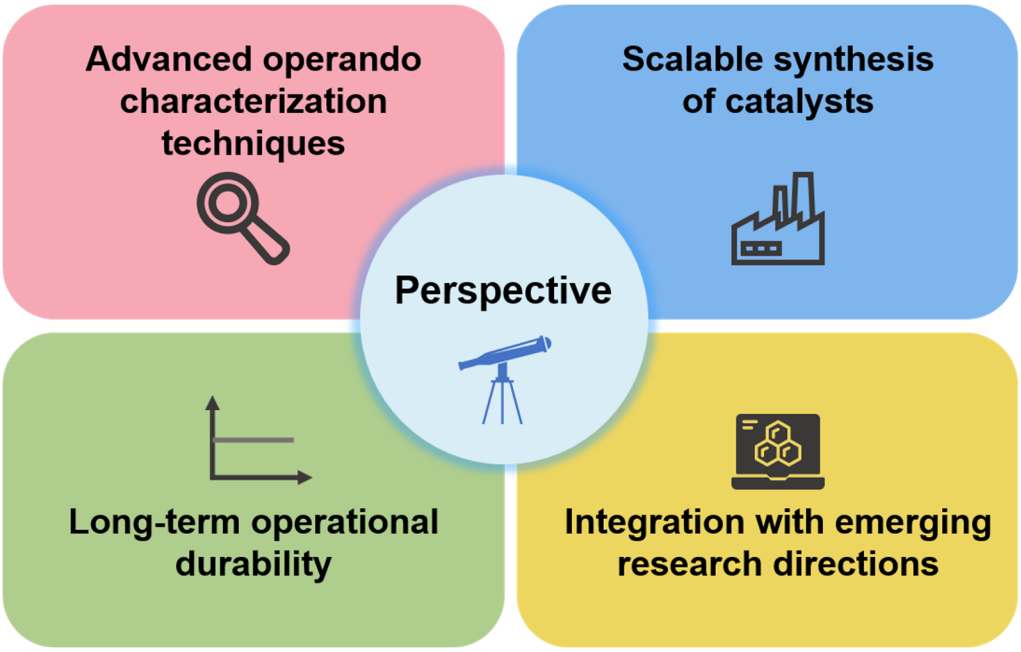

Figure 10. Perspectives on MOF-based CO_2RR catalysts development.

In summary, studies of MOF-based CO_2RR catalysts over the past decade have progressed from conceptual verification to mechanistic analysis and application-focused catalyst design. Ongoing development of operando characterizations, data-assisted catalyst development and industrially applicable reactors will promote further practical deployment of MOF catalysts in CO_2RR. In the near future, we anticipate that MOF-based catalysts will achieve further breakthroughs and contribute to the advancement of CO_2RR technology as well as the realization of carbon neutrality.

Author Contributions

H.D.: conceptualization, supervision, writing—reviewing and editing, funding acquisition; R.J.: data curation, writing—original draft preparation; X.Z.: writing—original draft preparation; Z.S.: writing—original draft preparation; T.W.: data curation; S.H.: data curation; R.L.: data curation; Z.L.: software; W.K.: writing—reviewing and editing, funding acquisition; F.H.: writing—reviewing and editing, funding acquisition; C.M.: writing—reviewing and editing, funding acquisition. All authors have read and agreed to the published version of the manuscript.

Funding

This work is supported by Shandong Provincial Natural Science Foundation (ZR2024QB370), National Natural Science Foundation of China (22272094), Central Guidance for Local Science and Technology Development Funds Project in Shandong Province (YDZX2025121) and State Key Laboratory of Analytical Chemistry for Life Science (SKLACLS2516).

Data Availability Statement

All data graphs in this manuscript are reproduced from previously published literature with corresponding citations provided.

Conflicts of Interest

The authors declare no conflict of interest.

Use of AI and AI-Assisted Technologies

No AI tools were utilized for this paper.

References

1. Yang, Z.; Li, X.; Cui, X.; et al. Integrated Strategies Toward the Capture and Electrochemical Conversion of Low-Concentration Carbon Dioxide. *Exploration* **2025**, *5*, e20240006. https://doi.org/10.1002/exp.20240006.
2. He, Z.; Xu, N.; Wang, Y.; et al. Electrode-resolved mechanisms governing performance and durability in zinc-air batteries. *Chem. Eng. J.* **2026**, *527*, 171444. https://doi.org/10.1016/j.cej.2025.171444.
3. Zeng, Z.; Li, L.; Smith, K.S.; et al. Quantifying Individual Electrode Polarization and Understanding the Interactive Phenomenon in Proton Exchange Membrane Fuel Cells. *J. Electrochem. Soc.* **2025**, *172*, 114507. https://doi.org/10.1149/1945-7111/ae18fb.
4. Zhu, W. Living bioreactive facades for visible carbon reduction in cities. *Nat. Cities* **2026**, *3*, 784–785. https://doi.org/10.1038/s44284-026-00502-3.
5. Dou, H.; Li, Y.; Wang, D.; et al. Confinement-enhanced photocatalytic CO_2 reduction: A comprehensive review of microstructural and electronic structural modulations. *Prog. Nat. Sci. Mater. Int.* **2026**, *36*, 752–784. https://doi.org/10.1016/j.pnsc.2026.06.008.
6. Kwon, W.; Kim, D.; Lee, Y.; et al. Advancements in Understanding Catalyst Reconstruction During Electrochemical CO_2 Reduction. *Exploration* **2025**, *5*, e20240019. https://doi.org/10.1002/exp.20240019.
7. Liu, S.; Wang, H.; Wang, X.; et al. Bi_2S_3/$In(OH)_3$ heterojunction for enhanced CO_2 electroreduction to formic acid. *Prog. Nat. Sci. Mater. Int.* **2024**, *34*, 1167–1172. https://doi.org/10.1016/j.pnsc.2024.10.009.
8. Xie, L.; Liu, Y.; Li, S.; et al. Phase and facet engineering for nanoscale catalyst discovery in electrochemical CO_2 reduction. *Nat. Synth.* **2026**, *5*, 489–505. https://doi.org/10.1038/s44160-026-01025-4.
9. Xue, J.; Yang, R.; Chen, Z. *In-Situ*/Operando Raman Spectroscopy Techniques for In-Depth Decoupling CO_2 Reduction Reaction Mechanisms. *Nano-Electrochem. Nano-Photochem.* **2025**, *1*, 2. https://doi.org/10.53941/nenp.2025.100002.
10. Du, H.; Fu, J.; Liu, L.X.; et al. Recent progress in electrochemical reduction of carbon monoxide toward multi-carbon products. *Mater. Today* **2022**, *59*, 182–199. https://doi.org/10.1016/j.mattod.2022.08.012.
11. Kim, J.H.; Hong, S.H.; Ahn, S.H.; et al. Recent Progress in Photocathode Interface Engineering for Photoelectrochemical CO_2 Reduction Reaction to C_1 or C_{2+} Products. *Exploration* **2025**, *5*, 70010. https://doi.org/10.1002/exp.20240014.
12. Du, H.; Liu, L.X.; Li, P.; et al. Enriching Reaction Intermediates in Multishell Structured Copper Catalysts for Boosted Propanol Electrosynthesis from Carbon Monoxide. *ACS Nano* **2023**, *17*, 8663–8670. https://doi.org/10.1021/acsnano.3c01516.
13. Ameen, S.; Abrar, A.; Wang, S.; et al. Thiol-directed synthesis of high-loading Ag nanoparticles on carbon for efficient and stable CO_2 electroreduction. *Prog. Nat. Sci. Mater. Int.* **2026**, *36*, 502–510. https://doi.org/10.1016/j.pnsc.2025.06.005.
14. Huang, J.; Yu, M.; Li, L.; et al. Radiation-induced divergent structural evolution of $Cu_2(OH)_2CO_3$ and its impact on CO_2 electroreduction. *Trans. Mater. Res.* **2026**, *2*, 100205. https://doi.org/10.1016/j.tramat.2026.100205.
15. Kong, W.; Zhu, D.; Zhang, Y.; et al. Electron Donor Coordinated Metal-Organic Framework to Enhance Photoelectrochemical Performance. *Angew. Chem. Int. Ed.* **2023**, *62*, e202308514. https://doi.org/10.1002/anie.202308514.
16. Du, H.; Liu, L.X.; Cai, Y.; et al. *In situ* formed N-containing copper nanoparticles: A high-performance catalyst toward carbon monoxide electroreduction to multicarbon products with high faradaic efficiency and current density. *Nanoscale* **2022**, *14*, 7262–7268. https://doi.org/10.1039/d2nr01226j.
17. Liu, J.; Burciaga, R.; Tang, S.; et al. Heterogeneous catalysis for the environment. *Innov. Mater.* **2024**, *2*, 100090. https://doi.org/10.59717/j.xinn-mater.2024.100090.

18. Qin, C.; Li, X.; Wang, T.; et al. Metal-Organic Frameworks-Based Copper Catalysts for CO_2 Electroreduction toward Multicarbon Products. *Exploration* **2025**, *5*, 270011. https://doi.org/10.1002/exp.70011.
19. Wang, Z.; Wang, H.; Wang, P.; et al. Application of MOFs driven by various energy sources for degradation the organic pollutants in water: A review. *Coord. Chem. Rev.* **2024**, *499*, 215506. https://doi.org/10.1016/j.ccr.2023.215506.
20. Xu, W.; Wu, Y.; Gu, W.; et al. Atomic-level design of metalloenzyme-like active pockets in metal–organic frameworks for bioinspired catalysis. *Chem. Soc. Rev.* **2024**, *53*, 137–162. https://doi.org/10.1039/d3cs00767g.
21. Yao, S.; Liu, J.; Tan, J.; et al. Conductive MOF-Based NiZn Dual Atom Catalyst for Boosted Photoreduction of Diluted CO_2: The Effects of Inert Sites. *Adv. Funct. Mater.* **2026**, *36*, e26031. https://doi.org/10.1002/adfm.202526031.
22. Sun, N.; Shah, S.S.A.; Lin, Z.; et al. MOF-Based Electrocatalysts: An Overview from the Perspective of Structural Design. *Chem. Rev.* **2025**, *125*, 2703–2792. https://doi.org/10.1021/acs.chemrev.4c00664.
23. Kong, W.; Liu, T.; Meng, X.; et al. Intrareticular Energy Transfer in Dual-Photosensitized Metal–Organic Frameworks to Enhance Photoelectrochemical Performance. *J. Am. Chem. Soc.* **2025**, *147*, 24976–24983. https://doi.org/10.1021/jacs.5c07699.
24. Huang, D.S.; Wang, Y.; Tang, Y.; et al. Embedding a self-supporting MOF-based molecular sieve membrane into an electrolyzer for boosting electroreduction of CO_2 in air and flue gas to HCOOH. *Natl. Sci. Rev.* **2025**, *12*, nwaf329. https://doi.org/10.1093/nsr/nwaf329.
25. Li, M.; Li, C.; Shi, Y.; et al. Embedding Metallosalen Active Sites in Zr-MOF for Enhanced Selective Syngas Production from CO_2 Photoreduction. *Angew. Chem. Int. Ed.* **2025**, *64*, e202510810. https://doi.org/10.1002/anie.202510810.
26. Lim, H.K.; Kwon, Y.; Kim, H.S.; et al. Insight into the Microenvironments of the Metal–Ionic Liquid Interface during Electrochemical CO_2 Reduction. *ACS Catal.* **2018**, *8*, 2420–2427. https://doi.org/10.1021/acscatal.7b03777.
27. Tao, Z.; Rooney, C.L.; Liang, Y.; et al. Accessing Organonitrogen Compounds via C–N Coupling in Electrocatalytic CO_2 Reduction. *J. Am. Chem. Soc.* **2021**, *143*, 19630–19642. https://doi.org/10.1021/jacs.1c10714.
28. Cui, M.; Xu, B.; Shi, X.; et al. Metal–organic framework-derived single-atom catalysts for electrocatalytic energy conversion applications. *J. Mater. Chem. A* **2024**, *12*, 18921–18947. https://doi.org/10.1039/d4ta03518f.
29. Ren, F.Y.; Hu, C.; Huang, W.B.; et al. Modulated Multicomponent Reaction Pathway by Pore-Confinement Effect in MOFs for Highly Efficient Catalysis of Low-Concentration CO_2. *Angew. Chem. Int. Ed.* **2025**, *64*, e202503898. https://doi.org/10.1002/anie.202503898.
30. Hu, H.; Liu, J.; Li, W.; et al. MOF-derived doped porous carbon-based catalysts for CO_2 electroreduction: Design, mechanisms, and scale-up. *Mater. Chem. Front.* **2026**, *10*, 888–921. https://doi.org/10.1039/d5qm00888c.
31. Li, P.; Yang, R.; Zhu, W. Quantum-dot-based catalysts for electrochemical CO_2 reduction: Structure–selectivity relationships and design principles. *J. Electroanal. Chem.* **2026**, *1015*, 120234. https://doi.org/10.1016/j.jelechem.2026.120234.
32. Wang, W.; Chen, D.; Li, F.; et al. Metal-organic-framework-based materials as platforms for energy applications. *Chem* **2024**, *10*, 86–133. https://doi.org/10.1016/j.chempr.2023.09.009.
33. Pan, F.; Yang, X.; O'Carroll, T.; et al. Carbon Catalysts for Electrochemical CO_2 Reduction toward Multicarbon Products. *Adv. Energy Mater.* **2022**, *12*, 2200586. https://doi.org/10.1002/aenm.202200586.
34. Wang, G.; Ma, Y.; Wang, J.; et al. Metal functionalization of two-dimensional nanomaterials for electrochemical carbon dioxide reduction. *Nanoscale* **2023**, *15*, 6456–6475. https://doi.org/10.1039/d3nr00484h.
35. Feaster, J.T.; Shi, C.; Cave, E.R.; et al. Understanding Selectivity for the Electrochemical Reduction of Carbon Dioxide to Formic Acid and Carbon Monoxide on Metal Electrodes. *ACS Catal.* **2017**, *7*, 4822–4827. https://doi.org/10.1021/acscatal.7b00687.
36. Rodrigues Pinto, M.; Vos, R.E.; Nagao, R.; et al. Electrolyte Effects on Electrochemical CO_2 Reduction Reaction at Sn Metallic Electrode. *J. Phys. Chem. C* **2024**, *128*, 21421–21429. https://doi.org/10.1021/acs.jpcc.4c06361.
37. Zhao, K.; Liu, Y.; Quan, X.; et al. CO_2 Electroreduction at Low Overpotential on Oxide-Derived Cu/Carbons Fabricated from Metal Organic Framework. *ACS Appl. Mater. Interfaces* **2017**, *9*, 5302–5311. https://doi.org/10.1021/acsami.6b15402.
38. Shah, S.S.A.; Javed, M.S.; Najam, T.; et al. Metal oxides for the electrocatalytic reduction of carbon dioxide: Mechanism of active sites, composites, interface and defect engineering strategies. *Coord. Chem. Rev.* **2022**, *471*, 214716. https://doi.org/10.1016/j.ccr.2022.214716.
39. Xiong, B.; Yang, Y.; Liu, J. HCOOH Electrosynthesis via Coelectrolytic Processes of CO_2 Reduction and CH_3OH Oxidation. *J. Phys. Chem. C* **2023**, *127*, 196–204. https://doi.org/10.1021/acs.jpcc.2c06031.
40. Lv, X.; Liu, Q.; Wang, J.; et al. Grain refining enables mixed Cu^+/Cu^0 states for CO_2 electroreduction to C_{2+} products at high current density. *Appl. Catal. B Environ.* **2023**, *324*, 122272. https://doi.org/10.1016/j.apcatb.2022.122272.
41. Nitopi, S.; Bertheussen, E.; Scott, S.B.; et al. Progress and Perspectives of Electrochemical CO_2 Reduction on Copper in Aqueous Electrolyte. *Chem. Rev.* **2019**, *119*, 7610–7672. https://doi.org/10.1021/acs.chemrev.8b00705.
42. Nie, X.; Esopi, M.R.; Janik, M.J.; et al. Selectivity of CO_2 Reduction on Copper Electrodes: The Role of the Kinetics of Elementary Steps. *Angew. Chem. Int. Ed.* **2013**, *52*, 2459–2462. https://doi.org/10.1002/anie.201208320.
43. Peterson, A.A.; Abild-Pedersen, F.; Studt, F.; et al. How copper catalyzes the electroreduction of carbon dioxide into hydrocarbon fuels. *Energy Environ. Sci.* **2010**, *3*, 1311–1315. https://doi.org/10.1039/c0ee00071j.

44. Wang, Y.; Han, P.; Lv, X.; et al. Defect and Interface Engineering for Aqueous Electrocatalytic CO_2 Reduction. *Joule* **2018**, *2*, 2551–2582. https://doi.org/10.1016/j.joule.2018.09.021.
45. Kibria, M.G.; Edwards, J.P.; Gabardo, C.M.; et al. Electrochemical CO_2 Reduction into Chemical Feedstocks: From Mechanistic Electrocatalysis Models to System Design. *Adv. Mater.* **2019**, *31*, 1807166. https://doi.org/10.1002/adma.201807166.
46. Xue, Y.; Guo, Y.; Cui, H.; et al. Catalyst Design for Electrochemical Reduction of CO_2 to Multicarbon Products. *Small Methods* **2021**, *5*, 2100736. https://doi.org/10.1002/smtd.202100736.
47. Ni, F.; Yang, H.; Wen, Y.; et al. N-modulated Cu^+ for efficient electrochemical carbon monoxide reduction to acetate. *Sci. China Mater.* **2020**, *63*, 2606–2612. https://doi.org/10.1007/s40843-020-1440-6.
48. Ma, W.; He, X.; Wang, W.; et al. Electrocatalytic reduction of CO_2 and CO to multi-carbon compounds over Cu-based catalysts. *Chem. Soc. Rev.* **2021**, *50*, 12897–12914. https://doi.org/10.1039/d1cs00535a.
49. Pérez-Gallent, E.; Figueiredo, M.C.; Calle-Vallejo, F.; et al. Spectroscopic Observation of a Hydrogenated CO Dimer Intermediate During CO Reduction on Cu(100) Electrodes. *Angew. Chem. Int. Ed.* **2017**, *56*, 3621–3624. https://doi.org/10.1002/anie.201700580.
50. Mamaghani, A.H.; Liu, J.; Zhang, Z.; et al. Promises of MOF-Based and MOF-Derived Materials for Electrocatalytic CO_2 Reduction. *Adv. Energy Mater.* **2024**, *14*, 2402278. https://doi.org/10.1002/aenm.202402278.
51. Kim, H.; An, H.; Kim, J.; et al. Dynamic Interface Engineering via Mechanistic Understanding of Copper Reconstruction in Electrochemical CO_2 Reduction Reaction. *J. Am. Chem. Soc.* **2026**, *148*, 6045–6056. https://doi.org/10.1021/jacs.5c16244.
52. Sudhakaran, A.; Prasad, D.; Saxena, M.; et al. Advances in electrochemical CO_2 reduction to CO for enabling A sustainable energy economy. *Prog. Mater. Sci.* **2026**, *159*, 101655. https://doi.org/10.1016/j.pmatsci.2026.101655.
53. Xie, F.; Zhan, S.; You, Z.; et al. Dual Electric Fields Enrich and Stabilize Intermediates for Efficient Electrochemical CO_2 Reduction to Multi-Carbon Products. *Adv. Funct. Mater.* **2026**, *36*, e17674. https://doi.org/10.1002/adfm.202517674.
54. Xiao, Y.; Lai, X.; Feng, J.; et al. Self-Refreshing Bi-Based Active Sites for Efficient and Durable Electrochemical CO_2 Reduction. *Adv. Funct. Mater.* **2026**, *36*, e23592. https://doi.org/10.1002/adfm.202523592.
55. Martín, A.J.; Larrazábal, G.O.; Pérez-Ramírez, J. Towards sustainable fuels and chemicals through the electrochemical reduction of CO_2: Lessons from water electrolysis. *Green Chem.* **2015**, *17*, 5114–5130. https://doi.org/10.1039/c5gc01893e.
56. Hao, S.; Elgazzar, A.; Zhang, S.K.; et al. Acid-humidified CO_2 gas input for stable electrochemical CO_2 reduction reaction. *Science* **2025**, *388*. https://doi.org/10.1126/science.adr3834. Erratum in *Science* **2026**, *391*. https://doi.org/10.1126/science.aeh0747.
57. Okatenko, V.; Loiudice, A.; Newton, M.A.; et al. Alloying as a Strategy to Boost the Stability of Copper Nanocatalysts during the Electrochemical CO_2 Reduction Reaction. *J. Am. Chem. Soc.* **2023**, *145*, 5370–5383. https://doi.org/10.1021/jacs.2c13437.
58. Álvarez-Gómez, J.M.; Varela, A.S. Review on Long-Term Stability of Electrochemical CO_2 Reduction. *Energy Fuels* **2023**, *37*, 15283–15308. https://doi.org/10.1021/acs.energyfuels.3c01847.
59. Hao, S.; Elgazzar, A.; Ravi, N.; et al. Improving the operational stability of electrochemical CO_2 reduction reaction via salt precipitation understanding and management. *Nat. Energy* **2025**, *10*, 266–277. https://doi.org/10.1038/s41560-024-01695-4.
60. Deng, W.; Zhang, L.; Li, L.; et al. Crucial Role of Surface Hydroxyls on the Activity and Stability in Electrochemical CO_2 Reduction. *J. Am. Chem. Soc.* **2019**, *141*, 2911–2915. https://doi.org/10.1021/jacs.8b13786.
61. Han, G.H.; Yoo, J.; Ha, J.; et al. How to Select Each Component of CO_2 Electrolyzers. *Exploration* **2025**, *5*, 20240025. https://doi.org/10.1002/exp.20240025.
62. Popović, S.; Smiljanić, M.; Jovanovič, P.; et al. Stability and Degradation Mechanisms of Copper-Based Catalysts for Electrochemical CO_2 Reduction. *Angew. Chem.* **2020**, *132*, 14844–14854. https://doi.org/10.1002/ange.202000617.
63. Lai, W.; Qiao, Y.; Wang, Y.; et al. Stability Issues in Electrochemical CO_2 Reduction: Recent Advances in Fundamental Understanding and Design Strategies. *Adv. Mater.* **2023**, *35*, e2306288. https://doi.org/10.1002/adma.202306288.
64. Xie, S.; Ma, W.; Wu, X.; et al. Photocatalytic and electrocatalytic transformations of C1 molecules involving C–C coupling. *Energy Environ. Sci.* **2021**, *14*, 37–89. https://doi.org/10.1039/d0ee01860k.
65. Rabinowitz, J.A.; Kanan, M.W. The future of low-temperature carbon dioxide electrolysis depends on solving one basic problem. *Nat. Commun.* **2020**, *11*, 5231. https://doi.org/10.1038/s41467-020-19135-8.
66. Jia, S.; Kong, L.X.; Guo, X.; et al. Construction of copper oxide/carbon nanocomposites derived from Cu-MOF and their application in electrochemical nitrite sensors. *Mater. Today Chem.* **2025**, *45*, 102707. https://doi.org/10.1016/j.mtchem.2025.102707.
67. Sikdar, N.; Junqueira, J.R.C.; Dieckhöfer, S.; et al. A Metal–Organic Framework derived $Cu_xO_yC_z$ Catalyst for Electrochemical CO_2 Reduction and Impact of Local pH Change. *Angew. Chem. Int. Ed.* **2021**, *60*, 23427–23434. https://doi.org/10.1002/anie.202108313.

68. Liu, C.; Zhang, X.D.; Huang, J.M.; et al. *In Situ* Reconstruction of Cu–N Coordinated MOFs to Generate Dispersive Cu/Cu_2O Nanoclusters for Selective Electroreduction of CO_2 to C_2H_4. *ACS Catal.* **2022**, *12*, 15230–15240. https://doi.org/10.1021/acscatal.2c04275.
69. Zhang, Y.; Zhang, L.; Feng, X.; et al. Trinuclear Cu(I) Metal–Organic Framework Inspires the Activation of *CO_2 Via Electrostatic Tension to Boost the Electrochemical Conversion of CO_2-to-Methanol. *Small* **2025**, *21*, e05892. https://doi.org/10.1002/smll.202505892.
70. Meng, J.; Wang, Y.; Jia, C.; et al. Ultra-stabilized Cu^{2+} sites in conductive MOF/t-Cu_2O interface for benchmark CO_2 reduction. *Nano Energy* **2025**, *141*, 111077. https://doi.org/10.1016/j.nanoen.2025.111077.
71. Hinogami, R.; Yotsuhashi, S.; Deguchi, M.; et al. Electrochemical Reduction of Carbon Dioxide Using a Copper Rubeanate Metal Organic Framework. *ECS Electrochem. Lett.* **2012**, *1*, H17–H19. https://doi.org/10.1149/2.001204eel.
72. Kumar, R.; Kumar, S.S.; Kulandainathan, M.A. Highly selective electrochemical reduction of carbon dioxide using Cu based metal organic framework as an electrocatalyst. *Electrochem. Commun.* **2012**, *25*, 70–73. https://doi.org/10.1016/j.elecom.2012.09.018.
73. Dong, L.Z.; Lu, Y.F.; Wang, R.; et al. Porous copper cluster-based MOF with strong cuprophilic interactions for highly selective electrocatalytic reduction of CO_2 to CH_4. *Nano Res.* **2022**, *15*, 10185–10193. https://doi.org/10.1007/s12274-022-4681-z.
74. Wang, Y.; Hou, P.; Wang, Z.; et al. Zinc Imidazolate Metal–Organic Frameworks (ZIF-8) for Electrochemical Reduction of CO_2 to CO. *ChemPhysChem* **2017**, *18*, 3142–3147. https://doi.org/10.1002/cphc.201700716.
75. Kang, X.; Zhu, Q.; Sun, X.; et al. Highly efficient electrochemical reduction of CO_2 to CH_4 in an ionic liquid using a metal–organic framework cathode. *Chem. Sci.* **2016**, *7*, 266–273. https://doi.org/10.1039/c5sc03291a.
76. Zhan, T.; Huang, J.; Yang, Y.; et al. Regulating the Microenvironment of Zn-Based Metal-Organic Framework for Enhanced CO_2 Electroreduction to Formate. *ChemCatChem* **2025**, *17*, e202401529. https://doi.org/10.1002/cctc.202401529.
77. Birdja, Y.Y.; Pérez-Gallent, E.; Figueiredo, M.C.; et al. Advances and challenges in understanding the electrocatalytic conversion of carbon dioxide to fuels. *Nat. Energy* **2019**, *4*, 732–745. https://doi.org/10.1038/s41560-019-0450-y.
78. Zhang, X.; Zhang, Y.; Li, Q.; et al. Highly efficient and durable aqueous electrocatalytic reduction of CO_2 to HCOOH with a novel bismuth–MOF: Experimental and DFT studies. *J. Mater. Chem. A* **2020**, *8*, 9776–9787. https://doi.org/10.1039/d0ta00384k.
79. Li, F.; Gu, G.H.; Choi, C.; et al. Highly stable two-dimensional bismuth metal-organic frameworks for efficient electrochemical reduction of CO_2. *Appl. Catal. B Environ.* **2020**, *277*, 119241. https://doi.org/10.1016/j.apcatb.2020.119241.
80. Qiu, X.F.; Zhu, H.L.; Huang, J.R.; et al. Highly Selective CO_2 Electroreduction to C_2H_4 Using a Metal–Organic Framework with Dual Active Sites. *J. Am. Chem. Soc.* **2021**, *143*, 7242–7246. https://doi.org/10.1021/jacs.1c01466.
81. Zhu, H.L.; Chen, H.Y.; Han, Y.X.; et al. A Porous π–π Stacking Framework with Dicopper(I) Sites and Adjacent Proton Relays for Electroreduction of CO_2 to C_{2+} Products. *J. Am. Chem. Soc.* **2022**, *144*, 13319–13326. https://doi.org/10.1021/jacs.2c04670.
82. Singh, A.K.; Gu, L.; Dutta Chowdhury, A.; et al. Exploring Ligand-Controlled C_2 Product Selectivity in Carbon Dioxide Reduction with Copper Metal–Organic Framework Nanosheets. *Inorg. Chem.* **2023**, *62*, 8803–8811. https://doi.org/10.1021/acs.inorgchem.3c00118.
83. Mao, X.; Gong, W.; Fu, Y.; et al. Computational Design and Experimental Validation of Enzyme Mimicking Cu-Based Metal–Organic Frameworks for the Reduction of CO_2 into C_2 Products: C–C Coupling Promoted by Ligand Modulation and the Optimal Cu–Cu Distance. *J. Am. Chem. Soc.* **2023**, *145*, 21442–21453. https://doi.org/10.1021/jacs.3c07108.
84. Zhang, M.; Zhu, W.; Liu, Z.; et al. Selective Sieving Effect of Multi-Atomic Bismuth Interfaces for Efficient Formate Electrosynthesis and Evolution at Industrial Current Density. *Angew. Chem.* **2025**, *137*, e202510206. https://doi.org/10.1002/ange.202510206.
85. Dou, S.; Song, J.; Xi, S.; et al. Boosting Electrochemical CO_2 Reduction on Metal–Organic Frameworks via Ligand Doping. *Angew. Chem. Int. Ed.* **2019**, *58*, 4041–4045. https://doi.org/10.1002/anie.201814711.
86. Lu, Y.; Zhong, H.; Li, J.; et al. sp-Carbon Incorporated Conductive Metal-Organic Framework as Photocathode for Photoelectrochemical Hydrogen Generation. *Angew. Chem. Int. Ed.* **2022**, *61*, e202208163. https://doi.org/10.1002/anie.202208163.
87. Wang, M.; Dong, R.; Feng, X. Two-dimensional conjugated metal–organic frameworks (2D *c*-MOFs): Chemistry and function for MOFtronics. *Chem. Soc. Rev.* **2021**, *50*, 2764–2793. https://doi.org/10.1039/d0cs01160f. Correction in *Chem. Soc. Rev.* **2022**, *51*, 793–794.
88. Yi, J.D.; Si, D.H.; Xie, R.; et al. Conductive Two-Dimensional Phthalocyanine-based Metal–Organic Framework Nanosheets for Efficient Electroreduction of CO_2. *Angew. Chem. Int. Ed.* **2021**, *60*, 17108–17114. https://doi.org/10.1002/anie.202104564.
89. Huang, Q.; Li, Q.; Liu, J.; et al. Disclosing CO_2 Activation Mechanism by Hydroxyl-Induced Crystalline Structure Transformation in Electrocatalytic Process. *Matter* **2019**, *1*, 1656–1668. https://doi.org/10.1016/j.matt.2019.07.003.

90. Jiang, X.; Li, H.; Xiao, J.; et al. Carbon dioxide electroreduction over imidazolate ligands coordinated with Zn(II) center in ZIFs. *Nano Energy* **2018**, *52*, 345–350. https://doi.org/10.1016/j.nanoen.2018.07.047.
91. Al-Attas, T.A.; Marei, N.N.; Yong, X.; et al. Ligand-Engineered Metal–Organic Frameworks for Electrochemical Reduction of Carbon Dioxide to Carbon Monoxide. *ACS Catal.* **2021**, *11*, 7350–7357. https://doi.org/10.1021/acscatal.1c01506.
92. Nwosu, U.; Siahrostami, S. Copper-based metal–organic frameworks for CO_2 reduction: Selectivity trends, design paradigms, and perspectives. *Catal. Sci. Technol.* **2023**, *13*, 3740–3761. https://doi.org/10.1039/d3cy00408b.
93. Liu, L.X.; Qin, C.; Deng, T.; et al. Cu MOF-based electrocatalysts for CO_2 reduction to multi-carbon products. *J. Mater. Chem. A* **2024**, *12*, 26421–26438. https://doi.org/10.1039/d4ta05059b.
94. Wang, L.; Jin, P.; Duan, S.; et al. *In-situ* incorporation of Copper(II) porphyrin functionalized zirconium MOF and TiO_2 for efficient photocatalytic CO_2 reduction. *Sci. Bull.* **2019**, *64*, 926–933. https://doi.org/10.1016/j.scib.2019.05.012.
95. Xiao, J.; You, S.; Huang, H.; et al. Regulation of Cu-MOF reconstruction for enhanced CO_2 electroreduction. *Appl. Catal. B Environ. Energy* **2025**, *375*, 125412. https://doi.org/10.1016/j.apcatb.2025.125412.
96. Kung, C.W.; Audu, C.O.; Peters, A.W.; et al. Copper Nanoparticles Installed in Metal–Organic Framework Thin Films are Electrocatalytically Competent for CO_2 Reduction. *ACS Energy Lett.* **2017**, *2*, 2394–2401. https://doi.org/10.1021/acsenergylett.7b00621.
97. Nam, D.H.; Shekhah, O.; Ozden, A.; et al. High-Rate and Selective CO_2 Electrolysis to Ethylene via Metal–Organic-Framework-Augmented CO_2 Availability. *Adv. Mater.* **2022**, *34*, 2207088. https://doi.org/10.1002/adma.202207088.
98. Xie, X.; Zhang, X.; Xie, M.; et al. Au-activated N motifs in non-coherent cupric porphyrin metal organic frameworks for promoting and stabilizing ethylene production. *Nat. Commun.* **2022**, *13*, 63. https://doi.org/10.1038/s41467-021-27768-6.
99. Mukhopadhyay, S.; Shimoni, R.; Liberman, I.; et al. Assembly of a Metal–Organic Framework (MOF) Membrane on a Solid Electrocatalyst: Introducing Molecular-Level Control Over Heterogeneous CO_2 Reduction. *Angew. Chem. Int. Ed.* **2021**, *60*, 13423–13429. https://doi.org/10.1002/anie.202102320.
100. Zhang, Y.; Chen, Y.; Wang, X.; et al. Self-Polarization Triggered Multiple Polar Units Toward Electrochemical Reduction of CO_2 to Ethanol with High Selectivity. *Angew. Chem.* **2023**, *135*, e202302241. https://doi.org/10.1002/ange.202302241.
101. Jiang, X.; Wu, H.; Chang, S.; et al. Boosting CO_2 electroreduction over layered zeolitic imidazolate frameworks decorated with Ag_2O nanoparticles. *J. Mater. Chem. A* **2017**, *5*, 19371–19377. https://doi.org/10.1039/c7ta06114e.
102. Li, X.; Guan, X.; Zhu, L.; et al. Electron transfer in catalysis: From fundamentals to strategies. *Chem. Soc. Rev.* **2025**, *54*, 11423–11467. https://doi.org/10.1039/d4cs00600c.
103. Samaniyan, M.; Mirzaei, M.; Khajavian, R.; et al. Heterogeneous Catalysis by Polyoxometalates in Metal–Organic Frameworks. *ACS Catal.* **2019**, *9*, 10174–10191. https://doi.org/10.1021/acscatal.9b03439.
104. Sun, M.L.; Wang, Y.R.; He, W.W.; et al. Efficient Electron Transfer from Electron-Sponge Polyoxometalate to Single-Metal Site Metal–Organic Frameworks for Highly Selective Electroreduction of Carbon Dioxide. *Small* **2021**, *17*, 2100762. https://doi.org/10.1002/smll.202100762.
105. Zhang, Y.; Zhang, X.Y.; Sun, W.Y. *In Situ* Carbon-Encapsulated Copper-Doped Cerium Oxide Derived from MOFs for Boosting CO_2-to-CH_4 Electro-Conversion. *ACS Catal.* **2023**, *13*, 1545–1553. https://doi.org/10.1021/acscatal.2c05538.
106. Yang, Z.; Wang, H.; Fei, X.; et al. MOF derived bimetallic CuBi catalysts with ultra-wide potential window for high-efficient electrochemical reduction of CO_2 to formate. *Appl. Catal. B Environ.* **2021**, *298*, 120571. https://doi.org/10.1016/j.apcatb.2021.120571.
107. Zhang, H.; Wang, T.; Wang, J.; et al. Surface-Plasmon-Enhanced Photodriven CO_2 Reduction Catalyzed by Metal-Organic-Framework-Derived Iron Nanoparticles Encapsulated by Ultrathin Carbon Layers. *Adv. Mater.* **2016**, *28*, 3703–3710. https://doi.org/10.1002/adma.201505187.
108. Ali, S.A.; Sadiq, I.; Ahmad, T. Synergizing Defect Chemistry and Single-Atom Catalysis: A Mechanistic Approach Toward Photochemical and Electrochemical CO_2RR Applications. *Adv. Energy Mater.* **2026**, *16*, e06535. https://doi.org/10.1002/aenm.202506535.
109. Li, M.; Wang, H.; Luo, W.; et al. Heterogeneous Single-Atom Catalysts for Electrochemical CO_2 Reduction Reaction. *Adv. Mater.* **2020**, *32*, 2001848. https://doi.org/10.1002/adma.202001848.
110. Wang, S.; Wang, L.; Wang, D.; et al. Recent advances of single-atom catalysts in CO_2 conversion. *Energy Environ. Sci.* **2023**, *16*, 2759–2803. https://doi.org/10.1039/d3ee00037k.
111. Han, A.; Wang, B.; Kumar, A.; et al. Recent Advances for MOF-Derived Carbon-Supported Single-Atom Catalysts. *Small Methods* **2019**, *3*, 1800471. https://doi.org/10.1002/smtd.201800471.
112. Wen, M.; Sun, N.; Jiao, L.; et al. Microwave-Assisted Rapid Synthesis of MOF-Based Single-Atom Ni Catalyst for CO_2 Electroreduction at Ampere-Level Current. *Angew. Chem. Int. Ed.* **2024**, *63*, e202318338. https://doi.org/10.1002/anie.202318338.
113. Zhang, E.; Wang, T.; Yu, K.; et al. Bismuth Single Atoms Resulting from Transformation of Metal–Organic Frameworks and Their Use as Electrocatalysts for CO_2 Reduction. *J. Am. Chem. Soc.* **2019**, *141*, 16569–16573. https://doi.org/10.1021/jacs.9b08259.

114. Chen, Z.; Zhang, X.; Liu, W.; et al. Amination strategy to boost the CO_2 electroreduction current density of M–N/C single-atom catalysts to the industrial application level. *Energy Environ. Sci.* **2021**, *14*, 2349–2356. https://doi.org/10.1039/d0ee04052e.
115. Zhao, K.; Nie, X.; Wang, H.; et al. Selective electroreduction of CO_2 to acetone by single copper atoms anchored on N-doped porous carbon. *Nat. Commun.* **2020**, *11*, 2455. https://doi.org/10.1038/s41467-020-16381-8.
116. Zhao, D.; Yu, K.; Song, P.; et al. Atomic-level engineering $Fe_1N_2O_2$ interfacial structure derived from oxygen-abundant metal–organic frameworks to promote electrochemical CO_2 reduction. *Energy Environ. Sci.* **2022**, *15*, 3795–3804. https://doi.org/10.1039/d2ee00878e.
117. Cao, T.; Dai, X.; Fu, Y.; et al. Coordination polymer-derived non-precious metal catalyst for propane dehydrogenation: Highly dispersed zinc anchored on N-doped carbon. *Appl. Surf. Sci.* **2023**, *607*, 155055. https://doi.org/10.1016/j.apsusc.2022.155055.
118. Zhou, D.; Li, X.; Shang, H.; et al. Atomic regulation of metal–organic framework derived carbon-based single-atom catalysts for the electrochemical CO_2 reduction reaction. *J. Mater. Chem. A* **2021**, *9*, 23382–23418. https://doi.org/10.1039/d1ta06915b.
119. Hu, C.; Wang, Y.; Chen, J.; et al. Main-Group Metal Single-Atomic Regulators in Dual-Metal Catalysts for Enhanced Electrochemical CO_2 Reduction. *Small* **2022**, *18*, 2201391. https://doi.org/10.1002/smll.202201391.
120. Jiao, L.; Zhu, J.; Zhang, Y.; et al. Non-Bonding Interaction of Neighboring Fe and Ni Single-Atom Pairs on MOF-Derived N-Doped Carbon for Enhanced CO_2 Electroreduction. *J. Am. Chem. Soc.* **2021**, *143*, 19417–19424. https://doi.org/10.1021/jacs.1c08050.
121. Li, S.; Guan, A.; Yang, C.; et al. Dual-Atomic Cu Sites for Electrocatalytic CO Reduction to C_{2+} Products. *ACS Mater. Lett.* **2021**, *3*, 1729–1737. https://doi.org/10.1021/acsmaterialslett.1c00543.
122. Jia, S.; Yang, L.; Wu, C.; et al. Machine Learning Reveals Role-Asymmetric Electronic Cooperation in Fe-Based Dual-Atom Catalysts. *Adv. Mater.* **2026**, *38*, e74833. https://doi.org/10.1002/adma.74833.
123. Miao, J.; Zhang, Y.; Ren, G.; et al. Dual-atom catalysts with unique electronic structures for energy-related electrocatalysis. *Sci. China Mater.* **2026**. https://doi.org/10.1007/s40843-026-4092-8.
124. Zang, Y.; Liu, T.; Wei, P.; et al. Selective CO_2 Electroreduction to Ethanol over a Carbon-Coated CuO_x Catalyst. *Angew. Chem. Int. Ed.* **2022**, *61*, e202209629. https://doi.org/10.1002/anie.202209629.
125. Cheng, Y.S.; Chu, X.P.; Ling, M.; et al. An MOF-derived copper@nitrogen-doped carbon composite: The synergistic effects of N-types and copper on selective CO_2 electroreduction. *Catal. Sci. Technol.* **2019**, *9*, 5668–5675. https://doi.org/10.1039/c9cy01131e.
126. Yang, F.; Deng, P.; Wang, Q.; et al. Metal–organic framework-derived cupric oxide polycrystalline nanowires for selective carbon dioxide electroreduction to C2 valuables. *J. Mater. Chem. A* **2020**, *8*, 12418–12423. https://doi.org/10.1039/d0ta03565c.
127. Wu, J.X.; Zhu, X.R.; Liang, T.; et al. Sn(101) Derived from Metal–Organic Frameworks for Efficient Electrocatalytic Reduction of CO_2. *Inorg. Chem.* **2021**, *60*, 9653–9659. https://doi.org/10.1021/acs.inorgchem.1c00946.
128. Sun, X.; Lu, L.; Zhu, Q.; et al. MoP Nanoparticles Supported on Indium-Doped Porous Carbon: Outstanding Catalysts for Highly Efficient CO2 Electroreduction. *Angew. Chem. Int. Ed.* **2018**, *57*, 2427–2431. https://doi.org/10.1002/anie.201712221.
129. Deng, P.; Yang, F.; Wang, Z.; et al. Metal–Organic Framework-Derived Carbon Nanorods Encapsulating Bismuth Oxides for Rapid and Selective CO_2 Electroreduction to Formate. *Angew. Chem. Int. Ed.* **2020**, *59*, 10807–10813. https://doi.org/10.1002/anie.202000657.
130. Yi, J.D.; Xie, R.; Xie, Z.L.; et al. Highly Selective CO_2 Electroreduction to CH_4 by *In Situ* Generated Cu_2O Single-Type Sites on a Conductive MOF: Stabilizing Key Intermediates with Hydrogen Bonding. *Angew. Chem.* **2020**, *132*, 23849–23856. https://doi.org/10.1002/ange.202010601.
131. Huo, H.; Wang, J.; Fan, Q.; et al. Cu-MOFs Derived Porous Cu Nanoribbons with Strengthened Electric Field for Selective CO_2 Electroreduction to C_{2+} Fuels. *Adv. Energy Mater.* **2021**, *11*, 2102447. https://doi.org/10.1002/aenm.202102447.
132. Cao, C.; Ma, D.D.; Gu, J.F.; et al. Metal–Organic Layers Leading to Atomically Thin Bismuthene for Efficient Carbon Dioxide Electroreduction to Liquid Fuel. *Angew. Chem. Int. Ed.* **2020**, *59*, 15014–15020. https://doi.org/10.1002/anie.202005577.
133. Yuan, W.W.; Wu, J.X.; Zhang, X.D.; et al. *In situ* transformation of bismuth metal–organic frameworks for efficient selective electroreduction of CO_2 to formate. *J. Mater. Chem. A* **2020**, *8*, 24486–24492. https://doi.org/10.1039/d0ta08092f.